Journal of Thermal Stresses

ISSN: 0149-5739 (Print) 1521-074X (Online) Journal homepage: http://www.tandfonline.com/loi/uths20

Thermal buckling analysis of FGM sandwich truncated conical shells reinforced by FGM stiffeners resting on elastic foundations using FSDT

Nguyen Dinh Duc, Kim Seung-Eock & Do Quang Chan

To cite this article: Nguyen Dinh Duc, Kim Seung-Eock & Do Quang Chan (2017): Thermal buckling analysis of FGM sandwich truncated conical shells reinforced by FGM stiffeners resting on elastic foundations using FSDT, Journal of Thermal Stresses, DOI: 10.1080/01495739.2017.1398623

To link to this article: https://doi.org/10.1080/01495739.2017.1398623

Published online: 11 Dec 2017.

JOURNAL OF THERMAL STRESSES
https://doi.org/10.1080/01495739.2017.1398623

Thermal buckling analysis of FGM sandwich truncated conical shells reinforced by FGM stiffeners resting on elastic foundations using FSDT

Nguyen Dinh Duc[a,b,c], Kim Seung-Eock[c], and Do Quang Chan[d]

[a]Advanced Materials and Structures Laboratory, VNU - University of Engineering and Technology, Cau Giay, Hanoi, Vietnam; [b]Infrastructure Engineering Program, Vietnam-Japan University, Tu Liem, Hanoi, Vietnam; [c]National Research Laboratory, Department of Civil and Environmental Engineering, Sejong University, Gwangjin-gu, Seoul, Korea; [d]Faculty of Technical Basis, University of Transport Technology, Thanh Xuan, Hanoi, Vietnam

ABSTRACT

This work presents an analytical approach to investigate the mechanical and thermal buckling of functionally graded materials sandwich truncated conical shells resting on Pasternak elastic foundations, subjected to thermal load and axial compressive load. Shells are reinforced by closely spaced stringers and rings, in which the material properties of shells and stiffeners are graded in the thickness direction following a general sigmoid law distribution and a general power law distribution. Four models of coated shell-stiffener arrangements are investigated. The change of spacing between stringers in the meridional direction also is taken into account. Two cases on uniform temperature rise and linear temperature distribution through the thickness of shell are considered. Using the first-order shear deformation theory, Lekhnitskii smeared stiffener technique and the adjacent equilibrium criterion, the linearization stability equations have been established. Approximate solution satisfies simply supported boundary conditions and Galerkin method is applied to obtain closed-form expression for determining the critical compression buckling load and thermal buckling load in cases uniform temperature rise and linear temperature distribution across the shell thickness. The effects of temperature, foundation, core layer, coating layer, stiffeners, material properties, dimensional parameters and semi-vertex angle on buckling behaviors of shell are shown.

ARTICLE HISTORY
Received 2 August 2017
Accepted 26 October 2017

KEYWORDS
Elastic foundations; first-order shear deformation theory; reinforced FGM stiffeners; sandwich truncated conical shell with FGM layers; thermal buckling

Introduction

Due to the high strength and thermal resistance, functionally graded material (FGM) conical shells were applied to many modern technique fields such as military aircraft propulsion system, and rocketry, underwater vehicles, missiles, tanks, pressure vessels, buildings of modern power plants, and other applications [1]. Therefore, the static and dynamic problems of FGM structures containing conical shells always attract the attention of many scientists. Chung and Chang [2] analyzed an elastic, rectangular, and simply supported FGM plate with medium thickness subjected to linear temperature change in the z-direction. Young's modulus and Poisson ratio of the FGM plates are assumed to remain constant throughout the entire plate. However, the coefficient of thermal expansion of the FGM plate varies continuously throughout the thickness direction in relation to the volume fraction of constituents defined by power-law, sigmoid, or exponential functions. The series solutions for the power-law FGM (P-FGM), sigmoid FGM (S-FGM), or exponential FGM (E-FGM) plates subjected to thermal loading are obtained based on the classical plate theory and Fourier series expansion. The analytical solutions for P-, S-, and

CONTACT Nguyen Dinh Duc ducnd@vnu.edu.vn Advanced Materials and Structures Laboratory, VNU - University of Engineering and Technology, Room 710, Building E3, 144 Xuan Thuy Street, Cau Giay, Hanoi, Vietnam.
Color versions of one or more of the figures in the article can be found online at www.tandfonline.com/uths.

E-FGM plates are verified by numerical results obtained with the finite element technique. Fazzolari [3] presented analysis of free vibration of functionally graded plates with temperature-dependent materials in thermal environment. In this study, two different volume fractions are considered: (i) P-FGM and (ii) S-FGM. The analysis is performed using advanced hierarchical higher-order equivalent single-layer plate theories developed using the method of power series expansion of displacement components. The modal characteristics of the P- and S-FGM plates are investigated while subjected to a temperature gradient. The governing equations are derived in their strong form using the principle of the virtual displacements and are solved in an exact sense using the Navier-type closed form solution. Lee et al. [4] presented a refined higher-order shear and normal deformation theory for E-, P-, and S-FGM plates on elastic foundation. In this study, the displacement field of the four-variable plate theory is modified by considering a thickness stretching effect. The number of unknown functions involved in the present theory is only five, as opposed to six or even greater numbers in the case of other shear and normal deformation theories. The present theory accounts for both shear deformation and thickness stretching effects by a parabolic variation of all displacements across the thickness, and satisfies the stress-free boundary conditions on the upper and lower surfaces of the plate. The equations of motion are derived from minimum total potential energy principle. Analytical solutions for the bending analysis are obtained for simply supported plates. It is assumed that the elastic medium is modeled as Pasternak elastic foundation. Naj et al. [5] studied thermal and mechanical instability of FGM truncated conical shells using the first-order shell theory. Bich et al. [6] investigated buckling of un-stiffened FGM conical panels under mechanical loads. Bagherizadeh et al. [7] investigated the mechanical buckling of FGM cylindrical shell that is embedded in an outer elastic medium and subjected to combined axial and radial compressive loads. A linear thermal buckling analysis of truncated hybrid FGM conical shells based on the classical shell theory using Sanders nonlinear kinematics equations was analyzed by Torabi et al. [8]. A linear buckling analysis for nanocomposite conical shells reinforced with single walled carbon nanotubes subjected to lateral pressure is presented by Jam and Kiani [9]. Free vibration analysis of open conical panels made of through-the-thickness FGMs is analyzed by Akbari et al. [10]. Tung [11] presented an analytical approach to investigate the nonlinear stability of clamped FGM shallow spherical shells and circular plates resting on elastic foundations, subjected to uniform external pressure and exposed to thermal environments. Sofiyev [12–14] investigated the linear stability and vibration of unstiffened FGM truncated conical shells with different boundary conditions. The same author [15] presented the buckling of FGM truncated conical shells subjected to axial compressive load and resting on Winkler–Pasternak foundations. Quan and Duc [16] presented analytical solutions for the nonlinear static and dynamic stability of imperfect eccentrically stiffened FGM (ES-FGM) higher-order shear deformable double curved shallow shell on elastic foundations in thermal environments. Mirzavand et al. [17] studied dynamic thermal post-buckling behavior of functionally graded cylindrical shells with surface-bonded piezoelectric actuators subjected to the combined action of thermal load and applied actuator voltage. Mahapatra et al. [18] reported the geometrically nonlinear thermomechanical transverse deflection responses of the functionally graded curved structure under the influence of nonlinear thermal field. Sofiyev and Kuruoglu [19] studied the nonlinear buckling behavior of FGM truncated conical shells surrounded by an elastic medium based on the classical shell theory and applying Galerkin method. Sofiyev and Kuruoglu [20] obtained a closed form of the solution for critical combined loads (combined effects of the axial load and lateral pressure or the axial load and hydrostatic pressure) of FGM truncated conical shell in the framework of the shear deformation theory. Tornabene and Viola [21] investigated static analysis of functionally graded doubly curved shells and panels of revolution applying the generalized differential quadrature method. Tornabene et al. [22] studied stress and strain recovery for functionally graded free-form and doubly-curved sandwich shells using higher-order equivalent single layer theory. Viola et al. [23] studied the static analysis of functionally graded conical shells and panels. In this study, a two-dimensional unconstrained third-order shear deformation theory is used for the evaluation of tangential and normal stresses in moderately thick functionally graded truncated conical shells and panels subjected to meridian, circumferential and normal uniform loadings. Nejad et al. [24] used the first-order shear deformation theory (FSDT) and multilayer method, a

semi-analytical solution has been performed for the purpose of elastic analysis of rotating thick truncated conical shells made of FGMs under nonuniform pressure. Based on the Donnell–Mushtari thin shell theory and the stiffeners smeared technique, Mecitoglu [25] studied the vibration characteristics of a stiffened truncated conical shell by the collocation method. The minimum weight design of axially loaded simply supported stiffened conical shells with natural frequency constraints is considered by Rao and Reddy [26]. The influence of placing the stiffeners inside as well as outside the conical shell on the optimum design is studied. The expressions for the critical axial (buckling) load and natural frequency of vibration of conical shell also are derived. Bagherizadeh et al. [27] presented the thermal buckling analysis of FG cylindrical shell on a Pasternak-type elastic foundation. Akbari et al. [28] studied thermal buckling of temperature-dependent FGM conical shells with arbitrary edge supports. Bifurcation behavior of heated conical shell made of a through-the-thickness FGM is investigated in the present research. Mirzaei and Kiani [29] studied thermal buckling of temperature dependent FG-carbon nanotubes reinforced composite conical shells. In this research, linear thermal buckling of a composite conical shell made from a polymeric matrix and reinforced with carbon nanotube fibers is investigated. Sabzikar Boroujerdy et al. [30] based on the Donnell theory of shells combined with the von Kármán type of geometrical nonlinearity, three coupled equilibrium equations for a through-the-thickness functionally graded cylindrical shell embedded in a two parameter Pasternak elastic foundation are obtained. Thermal bifurcation behavior of cross-ply laminated composite cylindrical shells embedded with shape memory alloy fibers is investigated by Asadi et al. [31]. Castro et al. [32] studied linear buckling predictions of un-stiffened laminated composite cylinders and cones under various loading and boundary conditions using semi-analytical models. Castro et al. [33] presented semi-analytical model to predict the non-linear behavior of unstiffened cylinders and cones considering initial geometric imperfections and various loads and boundary conditions is presented.

As can be seen, the above introduced works mainly related to unstiffened FGM structures. However, in practice, plates and shells including conical shells, usually reinforced by stiffeners system to provide the benefit of added load carrying capability with a relatively small additional weight. Thus, the study on static and dynamic behavior of these structures are significant practical problem. Najafizadeh et al. [34], with the linearized stability equations in terms of displacements studied buckling of FGM cylindrical shell reinforced by rings and stringers under axial compression. The stiffeners and skin, in their work, are assumed to be made of FGMs and its properties vary continuously through the thickness direction. The nonlinear buckling of the shells reinforced by stiffeners in thermal environment was considered by Duc and Quan [35] for the imperfect ES-FGM double curved thin shallow shells on elastic foundations. The nonlinear dynamic behavior of eccentrically stiffened functionally graded circular cylindrical thin shells under external pressure and surrounded by an elastic medium was studied by Dung and Nam [36]. Dung and Hoa [37] investigated the nonlinear buckling and post-buckling of functionally graded stiffened thin circular cylindrical shells surrounded by elastic foundations in thermal environments and under torsional load by analytical approach. Duc [38] presented an analytical investigation on nonlinear thermal dynamic behavior of imperfect functionally graded circular cylindrical shells eccentrically reinforced by outside stiffeners and surrounded by elastic foundations using the Reddy's third-order shear deformation shell theory in thermal environment. Material properties are graded in the thickness direction according to sigmoid power law distribution (S-FGM) in terms of the volume fractions of constituents with metal–ceramic–metal layers. Duc et al. [39] studied nonlinear dynamic analysis and vibration of eccentrically stiffened S-FGM elliptical cylindrical shells surrounded by elastic foundations in thermal environments.

For ES-FGM conical shells, studies on their buckling and vibration are still limited and they should be further studied. This may be attributed to the inherent complexity of governing equations of conical shell, as well as variable coefficient partial differential equations. Dung et al. [40] studied linear buckling of FGM thin truncated conical shells reinforced by homogeneous eccentrically stringers and rings subjected to axial compressive load and uniform external pressure load based on the smeared stiffeners technique and the classical shell theory. Dung et al. [41] investigated an analytical solution for buckling of an eccentrically stiffened sandwich truncated conical shell. In this study, the shell consists of two FGM

coating layers and a core layer which are metal or ceramic subjected to an axial compressive load and an external uniform pressure. Shells are reinforced by stringers and rings, in which the material properties of shells and stiffeners are graded in the thickness direction following a general sigmoid law distribution. Two models of coated shell-stiffener arrangements are investigated. Duc and Cong [42] investigated nonlinear thermal stability of ES-FGM truncated conical surrounded on elastic foundations based on the classical shell theory. Duc et al. [43] investigated the linear stability analysis of ES-FGM conical shell panels reinforced by mechanical and thermal loads on elastic foundations. The FGM conical shell is in thermal environment and both the panel and the stiffeners are deformed under temperature. The material properties of both the panels and stiffeners are assumed to be temperature-dependent.

As can be observed, the studies in Dung et al. [40, 41], Duc and Cong [42], and Duc et al. [43] were performed using the classical shell theory, so obtained results only are suitable for thin-walled conical shells. However, for thicker conical shells, it is necessary to use higher-order theories. Recently, there are some investigations on buckling of truncated conical shells using the FSDT [9, 10, 24, 32], but these structures are unstiffened conical shells.

Nowadays, in the world, the sandwich structures have become more popular, known as one of the principal elements of structure in aircraft, satellites, submarines, water-borne ballistic missiles, or in civil engineering. Their mechanical properties vary smoothly and continuously in preferred directions, that enable sandwich FGMs to avoid interface problems, as well as unexpected stress concentrations. However, the sandwich structures also have the mentionable properties, especially thermal and sound insulation. Sandwich structures find an increasing use in aerospace, naval, transportation, and other industries, in which stiff and lightweight structural components are required. Various theoretical models have been developed in the recent years to discuss the static and dynamic behavior of these structures. There are significant studies on the stability and vibration of layered FGM shells. Liew et al. [44] analyzed the nonlinear vibration of a three-layer coating-FGM-substrate based on the FSDT with the geometric nonlinearity in von Kármán sense. Alibeigloo and Liew [45] investigated the free vibration of sandwich cylindrical panel with FGM core using the three-dimensional theory of elasticity. The state space technique was used to obtain natural frequencies analytically in this work. Li and Batra [46] considered the buckling of a simply supported three-layer circular cylindrical shell under the axial compressive load. The inner and outer layers of the shell are comprised of the same homogenous and isotropic material, and the middle layer is made of FGM. Sofiyev and Kuruoglu [47] solved the problem on vibration and buckling of the cylindrical shell with FGM coatings in an elastic medium. Sofiyev [48] studied the vibration and buckling of sandwich cylindrical shells covered by different types of coatings, such as functionally graded, metal, and ceramic coatings and subjected to a uniform hydrostatic pressure using the FSDT. Najafov et al. [49] considered the linear and nonlinear vibrations of a truncated conical shell. Both internal and external surfaces are covered by functionally graded coatings. The theoretical formulation is based on the von Kármán–Donnell-type nonlinear kinematics. The basic equations are reduced to the ordinary differential equation depending on time with geometric nonlinearity using the Superposition and Galerkin methods. Soyev et al. [50] examined the stability of thin three-layered truncated conical shells containing a functionally graded (FG) layer subjected to non-uniform lateral pressure. Deniz [51] investigated response of a FG coated truncated conical shell subjected to an axial load by means of non-linear equations governing the finite deformations of the shell. Sofiyev [52] studied dynamic buckling of truncated conical shells with functionally graded coatings subjected to a time dependent axial load in the large deformation. The method of solution utilizes Superposition principle and Galerkin procedure. Temperature-dependent buckling analysis of sandwich truncated conical shells with FG facesheets was studied by Seidi et al. [53]. In this study, an improved high-order theory is presented for temperature-dependent buckling analysis of sandwich conical shell with thin functionally graded (FG) facesheets and homogenous soft core. Duc [54] studied the nonlinear dynamic response of higher-order shear deformable sandwich functionally graded circular cylindrical shells with outer surface-bonded piezoelectric actuator on elastic foundations subjected to thermo-electromechanical and damping loads. The sigmoid FGM shells are made of the metal–ceramic–metal layers with temperature-dependent material properties. The governing equations are established based on Reddy's third-order

shear deformation theory using the stress function, the Galerkin method and the fourth-order Runge–Kutta method. Duc and Quan considered nonlinear dynamic analysis of imperfect FGM double curved thin [55] and thick [56] shallow shells with temperature-dependent properties on elastic foundations also using Galerkin method.

To the best of the authors' knowledge, there is no analytical approach on the stability of FGM sandwich truncated conical shells subjected to thermal load and axial compressive load.

The new contribution of this article is to use the FSDT for investigating the stability of FGM sandwich truncated conical shells subjected to thermal load and axial compressive load. Shells are reinforced by closely spaced FGM stringers and rings. The material properties of shells and stiffeners are assumed to be graded in the thickness direction according to a general sigmoid law distribution and a general power law in terms of the volume fractions of the constituents. The change of spacing between stringers in the meridional direction are taken into account. Four models of coated shell-stiffener arrangements are investigated. The general formula for force and moment resultants of ES-FGM truncated conical shells are established correctly by the Lekhnitskii smeared stiffeners technique. By using the adjacent equilibrium criterion, the linearization stability equations are established. As a result of that, five variable coefficient partial differential equations are solved by Galerkin method. Two cases of uniform temperature rise and linear temperature distribution through the thickness of shell are considered. The closed-form expression for determining the critical buckling load, thermal buckling load and thermo-mechanical buckling load are obtained. The effects of various parameters such as the temperature, the foundation, the core layer, the coating layer, the stiffener, the semi-vertex angle, the volume fraction index of materials, and the dimensional parameters on stability of shell are analyzed.

FGM sandwich truncated conical shell model

Consider a FGM sandwich truncated conical shell of thickness h and semi-vertex angle β. The geometry of shell is shown in Figure 1, where L is the length, H is the height of the truncated conical shell, and R is its small base radius. The truncated cone is referred to a curvilinear coordinate system (x, θ, z) with origin is located in the middle surface of the shell, x is in the generatrix direction measured from the

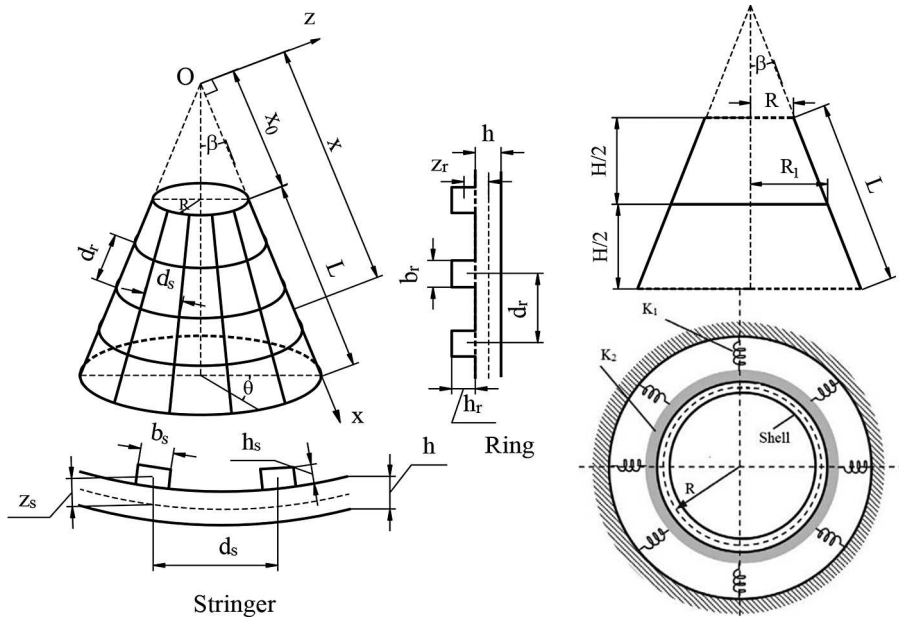

Figure 1. Geometry of eccentrically stiffened truncated conical shell surrounded by an elastic foundation.

vertex of conical shell, θ is in the circumferential direction and the axis z being perpendicular to the axis x, lies in the outwards normal direction of the cone. Also, x_0 indicates the distance from the vertex to small base of the shell. Assume that the shell consists of two coating layers and one core layer.

Furthermore, assume that the conical shell is stiffened eccentrically by closely spaced FGM longitudinal stringers and rings. To guarantee the continuity between the stiffener and shell, the stiffener side is taken to be pure-metal if it is located at metal-rich shell side and is pure-ceramic if it is located at ceramic-rich shell side. In this study, four models with eight cases are investigated, in which the material properties of shell and stiffeners are graded in the thickness direction with a general model of power law and general model of sigmoid law distribution as follows.

General model of sigmoid law

First model [1, 2, 4, 38] (FGM–Ceramic core–FGM conical shell, Figure 2a)

Case 1: FGM–Ceramic core–FGM conical shell and inside FGM stiffener.

Case 2: FGM–Ceramic core–FGM conical shell and outside FGM stiffener.
Second model (FGM–Metal core–FGM conical shell, Figure 2b)

Case 3: FGM–Metal core–FGM conical shell and inside FGM stiffener.

Case 4: FGM–Metal core–FGM conical shell and outside FGM stiffener.

General model of power law

Third model [1, 2, 4, 35] (Ceramic–FGM core–Metal conical shell, Figure 2c)

Case 5: Ceramic–FGM core–Metal conical shell and inside FGM stiffener.

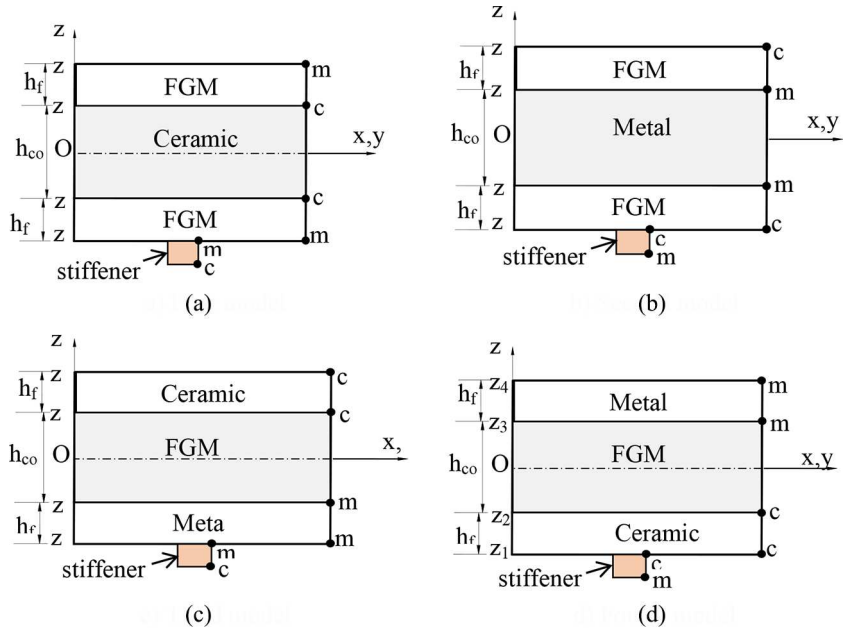

Figure 2. Four models of FGM sandwich truncated conical shell ($h = 2h_f + h_{co}$).

Case 6: Ceramic–FGM core–Metal conical shell and outside FGM stiffener.
Fourth model (Metal–FGM core–Ceramic conical shell, Figure 2d)

Case 7: Metal–FGM core–Ceramic conical shell and inside FGM stiffener.

Case 8: Metal–FGM core–Ceramic conical shell and outside FGM stiffener.

Theoretical formulation of FGM truncated conical shell

According to the Timoshenko–Mindlin assumption, the displacements at distance z from the middle surface of the shell, are represented in displacement components u, v, w of a point in the middle surface in the direction x, θ, and z, respectively [57]

$$u_x = u + z\phi_x, u_\theta = v + z\phi_\theta, u_z = w \tag{1}$$

in which ϕ_x, ϕ_θ are the rotations of a transverse normal about the θ and x-axis, respectively.

The strain–displacement relationship at the middle surface of the shell based on the FSDT taking into account the von Kármán geometrical nonlinearity is given by [1, 58, 59]

$$\begin{gathered}\varepsilon_{xm} = u_{,x} + \frac{1}{2}w_{,x}^2, \varepsilon_{\theta m} = \frac{1}{x\sin\beta}v_{,\theta} + \frac{u}{x} + \frac{w}{x}\cot\beta + \frac{1}{2x^2\sin^2\beta}w_{,\theta}^2 \\ \gamma_{x\theta m} = \frac{1}{x\sin\beta}u_{,\theta} - \frac{v}{x} + v_{,x} + \frac{1}{x\sin\beta}w_{,x}w_{,\theta}, \gamma_{xzm} = w_{,x} + \phi_x, \gamma_{\theta zm} = \frac{1}{x\sin\beta}w_{,\theta} + \phi_\theta\end{gathered} \tag{2}$$

$$k_x = \phi_{x,x}, k_\theta = \frac{1}{x\sin\beta}\phi_{\theta,\theta} + \frac{1}{x}\phi_x, k_{x\theta} = \frac{1}{2}\left[\phi_{\theta,x} + \frac{1}{x\sin\beta}\phi_{x,\theta} - \frac{1}{x}\phi_\theta\right] \tag{3}$$

where ε_{xm} and $\varepsilon_{\theta m}$ are the normal strains and $\gamma_{x\theta m}$ is the shear strain at the middle surface of the shell, and $\gamma_{xzm}, \gamma_{\theta zm}$ are the transverse shear strains; and k_x are the change of curvatures and twist, respectively.

The normal and shear strains at distance z from the middle surface of shell are of the form

$$\varepsilon_x = \varepsilon_{xm} + zk_x, \varepsilon_\theta = \varepsilon_{\theta m} + zk_\theta, \gamma_{x\theta} = \gamma_{x\theta m} + 2zk_{x\theta}, \gamma_{xz} = \gamma_{xzm}, \gamma_{\theta z} = \gamma_{\theta zm} \tag{4}$$

The stress–strain relations including temperature effects based on Hooke law is given by:
For the FGM conical shell

$$\begin{gathered}\sigma_x^{sh} = \frac{E_{sh}}{1-\nu^2}(\varepsilon_x + \nu\varepsilon_\theta) - \frac{E_{sh}\alpha_{sh}\Delta T(z)}{1-\nu}, \Delta T(z) = T - T_0 \\ \sigma_\theta^{sh} = \frac{E_{sh}}{1-\nu^2}(\varepsilon_\theta + \nu\varepsilon_x) - \frac{E_{sh}\alpha_{sh}\Delta T(z)}{1-\nu} \\ \sigma_{x\theta}^{sh} = \frac{E_{sh}}{2(1+\nu)}\gamma_{x\theta}, \sigma_{xz}^{sh} = \frac{E_{sh}}{2(1+\nu)}\gamma_{xzm}, \sigma_{\theta z}^{sh} = \frac{E_{sh}}{2(1+\nu)}\gamma_{\theta zm}\end{gathered} \tag{5}$$

For longitudinal stringers and rings, respectively

$$\sigma_x^{\mathrm{s}} = E_{\mathrm{s}}\varepsilon_x - E_{\mathrm{s}}\alpha_{\mathrm{s}}\Delta T(z), \sigma_\theta^{\mathrm{r}} = E_{\mathrm{r}}\varepsilon_\theta - E_{\mathrm{r}}\alpha_{\mathrm{r}}\Delta T(z) \tag{6}$$

where $\Delta T(z)$ denotes the change of environment temperature from thermal stress free initial state. Subscripts s and r denote longitudinal stringers and rings, respectively. The force and moment resultants

are expressed in terms of the stress components through the thickness as

$$N_i = \int_{-\frac{h}{2}}^{\frac{h}{2}} \sigma_i^{\mathrm{sh}} \mathrm{d}z + N_i^{\mathrm{st}}, \quad M_i = \int_{-\frac{h}{2}}^{\frac{h}{2}} z\sigma_i^{\mathrm{sh}} dz + M_i^{\mathrm{st}}, \quad (i = x, \theta)$$
$$N_{x\theta} = \int_{-\frac{h}{2}}^{\frac{h}{2}} \sigma_{x\theta}^{\mathrm{sh}} \mathrm{d}z, \quad M_{x\theta} = \int_{-\frac{h}{2}}^{\frac{h}{2}} x\sigma_{x\theta}^{\mathrm{sh}} \mathrm{d}z, \quad Q_x = \frac{5}{6}\int_{-\frac{h}{2}}^{\frac{h}{2}} \sigma_{xz}^{\mathrm{sh}} \mathrm{d}z, \quad Q_\theta = \frac{5}{6}\int_{-\frac{h}{2}}^{\frac{h}{2}} \sigma_{\theta z}^{\mathrm{sh}} \mathrm{d}z \tag{7}$$

where $N_i^{\mathrm{st}}, M_i^{\mathrm{st}}$ are force resultants and moment resultants of stiffeners, respectively. In this article, it is assumed that the thermal stress of stiffeners is negligible, therefore, we can ignore it.

Setting Eqs. (2)–(6) into Eq. (7) and using Lekhnitskii smeared stiffener technique, and taking into account the change of spacing between stringers in the meridional direction, after integrating the above stress–strain equations and their moments through the thickness of the shell, the expressions for force and moment resultants, and transverse force resultants of an ES-FGM conical shell are given by

$$\begin{aligned} N_x &= \left[A_{11} + \frac{E_{1\mathrm{s}} b_{\mathrm{s}}}{d_{\mathrm{s}}(x)}\right]\varepsilon_{xm} + A_{12}\varepsilon_{\theta m} + [B_{11} + c_1(x)]\, k_x + B_{12}k_\theta + \Phi_{\mathrm{a}} \\ N_\theta &= A_{12}\varepsilon_{xm} + \left[A_{22} + \frac{E_{1r} b_r}{d_r}\right]\varepsilon_{\theta m} + B_{12}k_x + (B_{22} + c_2)\, k_\theta + \Phi_a \\ N_{x\theta} &= A_{66}\gamma_{x\theta m} + 2B_{66}k_{x\theta} \end{aligned} \tag{8}$$

$$\begin{aligned} M_x &= [B_{11} + c_1(x)]\,\varepsilon_{xm} + B_{12}\varepsilon_{\theta m} + \left[D_{11} + \frac{E_{3\mathrm{s}} b_{\mathrm{s}}}{d_{\mathrm{s}}(x)}\right]k_x + D_{12}k_\theta + \Phi_{\mathrm{b}}, \\ M_\theta &= B_{12}\varepsilon_{xm} + (B_{22} + c_2)\,\varepsilon_{\theta m} + D_{12}k_x + \left[D_{22} + \frac{E_{3\mathrm{r}} b_{\mathrm{r}}}{d_{\mathrm{r}}}\right]k_\theta + \Phi_{\mathrm{b}} \\ M_{x\theta} &= B_{66}\gamma_{x\theta m} + 2D_{66}k_{x\theta} \end{aligned} \tag{9}$$

$$Q_x = A_{44}\gamma_{xzm} = A_{44}\left(w_{,x} + \phi_x\right), \quad Q_\theta = A_{55}\gamma_{\theta zm} = A_{55}\left[\frac{1}{x\sin\beta}w_{,\theta} + \phi_\theta\right] \tag{10}$$

where the coefficients E_i, $E_{i\mathrm{s}}$, $E_{i\mathrm{r}}$, $c_1(x)$, c_2, $d_{\mathrm{s}}(x)$, d_{r}, b_{s}, b_{r}, n_{s}, n_{r}, A_{ij}, B_{ij}, D_{ij}, Φ_{a}, Φ_{b}, are defined in Appendix A and b_s and b_r are the width of stringer and ring, respectively.

The reaction–deflection relation of Pasternak foundation model is expressed by

$$q_{\mathrm{f}} = K_1 w - K_2\left(\frac{\partial^2 w}{\partial x^2} + \frac{1}{x}\frac{\partial w}{\partial x} + \frac{1}{x^2\sin^2\beta}\frac{\partial^2 w}{\partial\theta^2}\right) \tag{11}$$

in which K_1 (N/m^3) is the Winkler foundation stiffness and K_2 (N/m) is the shear subgrade modulus of the Pasternak foundation model.

The nonlinear equilibrium equations of truncated conical shells surrounded by elastic foundation according to FSDT, are of the form [42, 57–59]

$$xN_{x,x} + \frac{1}{\sin\beta}N_{x\theta,\theta} + N_x - N_\theta = 0 \tag{12a}$$

$$\frac{1}{\sin\beta}N_{\theta,\theta} + xN_{x\theta,x} + 2N_{x\theta} = 0 \tag{12b}$$

$$xM_{x,xx} + 2M_{x,x} + \frac{2}{\sin\beta}M_{x\theta,x\theta} + \frac{2}{x\sin\beta}M_{x\theta,\theta} + \frac{1}{x\sin^2\beta}M_{\theta,\theta\theta} - M_{\theta,x} - N_\theta \cot\beta$$
$$+ \left[xN_x w_{,x} + \frac{1}{\sin\beta}N_{x\theta}w_{,\theta}\right]_{,x} + \frac{1}{\sin\beta}\left[N_{x\theta}w_{,x} + \frac{1}{x\sin\beta}N_\theta w_{,\theta}\right]_{,\theta}$$
$$= xK_1 w - xK_2\left(\frac{\partial^2 w}{\partial x^2} + \frac{1}{x}\frac{\partial w}{\partial x} + \frac{1}{x^2\sin^2\beta}\frac{\partial^2 w}{\partial\theta^2}\right) \tag{12c}$$

$$(x\sin\beta M_x)_{,x} + M_{x\theta,\theta} - M_\theta \sin\beta - x\sin\beta Q_x = 0 \tag{12d}$$

$$(x\sin\beta M_{x\theta})_{,x} + M_{\theta,\theta} + M_{x\theta}\sin\beta - x\sin\beta Q_\theta = 0 \tag{12e}$$

Linearization stability equations

The stability equations of conical shell are derived using the adjacent equilibrium criterion. Based on this criterion, each of the displacement components on the primary equilibrium path are perturbed infinitesimally to establish a new equilibrium configuration. The components of displacement field at the new adjacent equilibrium configuration may be written as [57]

$$u = u_0 + u_1, \quad v = v_0 + v_1, \quad w = w_0 + w_1, \quad \phi_x = \phi_{x0} + \phi_{x1}, \quad \phi_\theta = \phi_{\theta 0} + \phi_{\theta 1} \tag{13}$$

Similarly, the force and moment resultants of a neighboring state may be related to the state of equilibrium as [57]

$$\begin{aligned} &N_x = N_{x0} + N_{x1}, \quad N_\theta = N_{\theta 0} + N_{\theta 1}, \quad N_{x\theta} = N_{x\theta 0} + N_{x\theta 1}, \quad Q_x = Q_{x0} + Q_{x1} \\ &Q_\theta = Q_{\theta 0} + Q_{\theta 1}, \quad M_x = M_{x0} + M_{x1}, \quad M_\theta = M_{\theta 0} + M_{\theta 1}, \quad M_{x\theta} = M_{x\theta 0} + M_{x\theta 1} \end{aligned} \tag{14}$$

where terms with 0 subscripts correspond to the u_0, v_0, w_0 displacements and those with 1 subscripts represents the portions of increments of force and moment resultants that are linear in u_1, v_1, and w_1. The substitution of Eqs. (13) and (14) into Eqs. (12a)–(12e) and note that the terms in the resulting equations with subscript 0 satisfy the equilibrium equations and therefore drop out of the equations, and the nonlinear terms with the subscript 1 are ignored because they are small compared to the linear terms, the remaining terms form the stability equations as follows [42, 57]:

$$xN_{x1,x} + \frac{1}{\sin\beta}N_{x\theta 1,\theta} + N_{x1} - N_{\theta 1} = 0 \tag{15a}$$

$$\frac{1}{\sin\beta}N_{\theta 1,\theta} + xN_{x\theta 1,x} + 2N_{x\theta 1} = 0 \tag{15b}$$

$$xM_{x1,xx} + 2M_{x1,x} + \frac{2}{\sin\beta}M_{x\theta 1,x\theta} + \frac{2}{x\sin\beta}M_{x\theta 1,\theta} + \frac{1}{x\sin^2\beta}M_{\theta 1,\theta\theta} - M_{\theta 1,x}$$
$$- N_{\theta 1}\cot\beta + \left[xN_{x0}w_{1,x} + \frac{1}{\sin\beta}N_{x\theta 0}w_{1,\theta}\right]_{,x} + \frac{1}{\sin\beta}\left[N_{x\theta 0}w_{1,x} + \frac{1}{x\sin\beta}N_{\theta 0}w_{1,\theta}\right]_{,\theta}$$
$$- xK_1 w_1 + xK_2\left(\frac{\partial^2 w_1}{\partial x^2} + \frac{1}{x}\frac{\partial w_1}{\partial x} + \frac{1}{x^2\sin^2\beta}\frac{\partial^2 w_1}{\partial\theta^2}\right) = 0 \tag{15c}$$

$$x\sin\beta M_{x1,x} + \sin\beta M_{x1} + M_{x\theta 1,\theta} - M_{\theta 1}\sin\beta - x\sin\beta Q_{x1} = 0 \tag{15d}$$

$$x\sin\beta M_{x\theta 1,x} + 2\sin\beta M_{x\theta 1} + M_{\theta 1,\theta} - x\sin\beta Q_{\theta 1} = 0 \tag{15e}$$

where the force and moment resultants for the subscript 1 are defined by

$$\begin{aligned}
N_{x1} &= \left[A_{11} + \frac{E_{1s}b_s}{d_s(x)}\right]\varepsilon_{xm1} + A_{12}\varepsilon_{\theta m1} + [B_{11} + c_1(x)]\,k_{x1} + B_{12}k_{\theta 1}\\
N_{\theta 1} &= A_{12}\varepsilon_{xm1} + \left[A_{22} + \frac{E_{1r}b_r}{d_r}\right]\varepsilon_{\theta m1} + B_{12}k_{x1} + (B_{22} + c_2)\,k_{\theta 1}\\
N_{x\theta 1} &= A_{66}\gamma_{x\theta m1} + 2B_{66}k_{x\theta 1}
\end{aligned} \tag{16}$$

$$\begin{aligned}
M_{x1} &= [B_{11} + c_1(x)]\,\varepsilon_{xm1} + B_{12}\varepsilon_{\theta m1} + \left[D_{11} + \frac{E_{3s}b_s}{d_s(x)}\right]k_{x1} + D_{12}k_{\theta 1}\\
M_{\theta 1} &= B_{12}\varepsilon_{xm1} + (B_{22} + c_2)\,\varepsilon_{\theta m1} + D_{12}k_{x1} + \left[D_{22} + \frac{E_{3r}b_r}{d_r}\right]k_{\theta 1}\\
M_{x\theta 1} &= B_{66}\gamma_{x\theta m1} + 2D_{66}k_{x\theta 1}
\end{aligned} \tag{17}$$

$$Q_{x1} = A_{44}\gamma_{xzm1} = A_{44}\left(w_{1,x} + \phi_{x1}\right), \quad Q_{\theta 1} = A_{55}\gamma_{\theta zm1} = A_{55}\left[\frac{1}{x\sin\beta}w_{1,\theta} + \phi_{\theta 1}\right] \tag{18}$$

and the linear form of the strains and curvatures and twist in terms of the displacement components are of the form

$$\begin{aligned}
&\varepsilon_{xm1} = u_{1,x}, \quad \varepsilon_{\theta m1} = \frac{1}{x\sin\beta}v_{1,\theta} + \frac{u_1}{x} + \frac{w_1}{x}\cot\beta, \quad \gamma_{x\theta m1} = \frac{1}{x\sin\beta}u_{1,\theta} - \frac{v_1}{x} + v_{1,x}\\
&\gamma_{xzm1} = w_{1,x} + \phi_{x1}, \quad \gamma_{\theta zm1} = \frac{1}{x\sin\beta}w_{1,\theta} + \phi_{\theta 1}
\end{aligned} \tag{19}$$

$$k_{x1} = \phi_{x1,x}, \quad k_{\theta 1} = \frac{1}{x\sin\beta}\phi_{\theta 1,\theta} + \frac{1}{x}\phi_{x1}, \quad k_{x\theta 1} = \frac{1}{2}\left[\phi_{\theta 1,x} + \frac{1}{x\sin\beta}\phi_{x1,\theta} - \frac{1}{x}\phi_{\theta 1}\right] \tag{20}$$

Setting Eqs. (16)–(18) into the Eqs. (15a)–(15e), taking into account Eqs. (19) and (20), we obtain a system of the linearization stability equations in terms of displacement components u_1, v_1, w_1 and $\phi_{x1}, \phi_{\theta 1}$ as follows:

$$\Delta_1 \equiv S_{11}(u_1) + S_{12}(v_1) + S_{13}(w_1) + S_{14}(\phi_{x1}) + S_{15}(\phi_{\theta 1}) = 0 \tag{21}$$

$$\Delta_2 \equiv S_{21}(u_1) + S_{22}(v_1) + S_{23}(w_1) + S_{24}(\phi_{x1}) + S_{25}(\phi_{\theta 1}) = 0 \tag{22}$$

$$\begin{aligned}
\Delta_3 \equiv\ & S_{31}(u_1) + S_{32}(v_1) + (S_{33} + S_{37}K_1 + S_{38}K_2)(w_1) + N^{\wedge}_{x0}S_{36}(w_1)\\
&+ S_{34}(\phi_{x1}) + S_{35}(\phi_{\theta 1}) = 0
\end{aligned} \tag{23}$$

$$\Delta_4 \equiv S_{41}(u_1) + S_{42}(v_1) + S_{43}(w_1) + S_{44}(\phi_{x1}) + S_{45}(\phi_{\theta 1}) = 0 \tag{24}$$

$$\Delta_5 \equiv S_{51}(u_1) + S_{52}(v_1) + S_{53}(w_1) + S_{54}(\phi_{x1}) + S_{55}(\phi_{\theta 1}) = 0 \tag{25}$$

where S_{ij} are differential operators can be found in Appendix B.

The system of Eqs. (21)–(25) are the couple set of five variable coefficient partial differential equations. It is used to analyze the stability and find the critical buckling load, thermal buckling load and thermomechanical buckling load of ES-FGM truncated conical shells. This system is more complex than the system of stability equations of plates or cylindrical shells. This is main reason why the buckling

investigation of ES-FGM truncated conical shells still is limited. In this article, the Galerkin method was used to solve these problems.

Thermal buckling analysis of ES-FGM truncated conical shells only subjected to thermal loads

Prebuckling thermal state

Consider an ES-FGM truncated conical shell only subjected to symmetric thermal loads. In this case, according to Naj et al. [5] and Torabi et al. [8] for finding pre-buckling force resultants $N_{x0}, N_{\theta 0}, N_{x\theta 0}$, it is necessary to solve equilibrium equations of the shell in membrane state. For this aim, all the moment, transverse force resultants and deflection terms must be set equal to zero in Eqs. (15a)–(15e). It leads to

$$N_{x\theta 0} = 0, \quad x\frac{\mathrm{d}N_{x0}}{\mathrm{d}x} + N_{x0} - N_{\theta 0} = 0, \quad -N_{\theta 0}\cot\beta = 0 \tag{26}$$

Solving this system with the boundary condition $N_{x0} = \Phi_a$ at $x = x_0 + L$, we obtain [5, 42]

$$N_{x0} = \frac{x_0 + L}{x}\Phi_a, \quad N_{x\theta 0} = 0, \quad N_{\theta 0} = 0 \tag{27}$$

Setting $N_{x0}^{\wedge} = xN_{x0}$ and noting Eq. (27), leads to

$$N_{x0}^{\wedge} = (x_0 + L)\,\Phi_{\mathrm{a}}. \tag{28}$$

Galerkin method for determining critical thermal buckling load

This work considers a conical shell with the simply supported conditions at both ends. Then the boundary conditions in this case, are expressed by Jam and Kiani [9] and Akbari et al. [10] as

$$N_{x1} = v_1 = w_1 = \phi_{\theta 1} = M_{x1} = 0 \quad \text{at } x = x_0,\ x_0 + L \tag{29}$$

The approximate solution satisfying the abovementioned boundary conditions may be found in the form

$$\begin{aligned} u_1 &= A\cos\frac{m\pi\,(x - x_0)}{L}\sin n\theta, \quad v_1 = B\sin\frac{m\pi\,(x - x_0)}{L}\cos n\theta \\ w_1 &= C\sin\frac{m\pi\,(x - x_0)}{L}\sin n\theta, \quad \phi_{x1} = \Phi_1\cos\frac{m\pi\,(x - x_0)}{L}\sin n\theta \\ \phi_{\theta 1} &= \Phi_2\frac{1}{x\sin\alpha}\sin\frac{m\pi\,(x - x_0)}{L}\cos n\theta \end{aligned} \tag{30}$$

where m is the number of half-waves in the generatrix direction and n is the number of full-waves in the circumferential direction of the shell, and A, B, C, and Φ_1, Φ_2 are constant coefficients.

As can be seen the boundary conditions $v_1 = 0, w_1 = 0$, and $\phi_{\theta 1} = 0$ at $x = x_0, x_0 + L$ are satisfied exactly, but $N_{x1} = 0$ and $M_{x1} = 0$ at $x = x_0, x_0 + L$ are fulfilled on the average sense as [47, 60]

$$\int_0^{2\pi}\left(\frac{\partial N_{x1}}{\partial x}\right)_{x=x_0,x_0+L}\mathrm{d}\theta = 0 \quad \text{and} \quad \int_0^{2\pi}\left(\frac{\partial M_{x1}}{\partial x}\right)_{x=x_0,x_0+L}\mathrm{d}\theta = 0$$

As above emphasized, it is difficult to use the trial function (30) and Eqs. (21)–(25) to obtain directly closed-form of buckling load. Therefore, a different procedure is presented here. Because $x_0 \le x \le x_0 + L$; $0 \le \theta \le 2\pi$ and for sake of convenience in integration, Eqs. (21), (22), and (24) are multiplied by x; Eqs. (23) and (24) by x^2 and the corresponding eigenfunctions, then applying Galerkin method for

the resulting equations, the following expressions are obtained

$$\int_{x_0}^{x_0+L}\int_0^{2\pi} x\Delta_1 \cos\frac{m\pi\,(x-x_0)}{L}\sin n\theta\cdot x\sin\beta\,\mathrm{d}\theta\,\mathrm{d}x = 0 \tag{31a}$$

$$\int_{x_0}^{x_0+L}\int_0^{2\pi} x\Delta_2 \sin\frac{m\pi\,(x-x_0)}{L}\cos n\theta\cdot x\sin\beta\,\mathrm{d}\theta\,\mathrm{d}x = 0 \tag{31b}$$

$$\int_{x_0}^{x_0+L}\int_0^{2\pi} x^2\Delta_3 \sin\frac{m\pi\,(x-x_0)}{L}\sin n\theta\cdot x\sin\beta\,\mathrm{d}\theta\,\mathrm{d}x = 0 \tag{31c}$$

$$\int_{x_0}^{x_0+L}\int_0^{2\pi} x\Delta_4 \cos\frac{m\pi\,(x-x_0)}{L}\sin n\theta\cdot x\sin\beta\,\mathrm{d}\theta\,\mathrm{d}x = 0 \tag{31d}$$

$$\int_{x_0}^{x_0+L}\int_0^{2\pi} x^2\Delta_5\frac{1}{x\sin\beta}\sin\frac{m\pi\,(x-x_0)}{L}\cos n\theta\cdot x\sin\beta\,\mathrm{d}\theta\,\mathrm{d}x = 0 \tag{31e}$$

Substituting Eq. (30) into Eqs. (31a)–(31e) and integrating those expressions, after series calculations and rearrangements, we obtain

$$L_{11}A + L_{12}B + L_{13}C + L_{14}\Phi_1 + L_{15}\Phi_2 = 0 \tag{32a}$$

$$L_{21}A + L_{22}B + L_{23}C + L_{24}\Phi_1 + L_{25}\Phi_2 = 0 \tag{32b}$$

$$L_{31}A + L_{32}B + \left(L_{33} + N_{x0}^{\wedge}L_{36} + K_1L_{37} + K_2L_{38}\right)C + L_{34}\Phi_1 + L_{35}\Phi_2 = 0 \tag{32c}$$

$$L_{41}A + L_{42}B + L_{43}C + L_{44}\Phi_1 + L_{45}\Phi_2 = 0 \tag{32d}$$

$$L_{51}A + L_{52}B + L_{53}C + L_{54}\Phi_1 + L_{55}\Phi_2 = 0 \tag{32e}$$

where the coefficients L_{ij} are given in Appendix C.

Because the Eqs. (32a)–(32e) is a system of linear homogeneous equations for A, B, C and Φ_1, Φ_2. So for the nontrivial solution, the determinant of its coefficient matrix must be to zero i.e.,

$$\begin{vmatrix} L_{11} & L_{12} & L_{13} & L_{14} & L_{15} \\ L_{21} & L_{22} & L_{23} & L_{24} & L_{25} \\ L_{31} & L_{32} & \left(L_{33} + N_{x0}^{\wedge}L_{36} + K_1L_{37} + K_2L_{38}\right) & L_{34} & L_{35} \\ L_{41} & L_{42} & L_{43} & L_{44} & L_{45} \\ L_{51} & L_{52} & L_{53} & L_{54} & L_{55} \end{vmatrix} = 0$$

Developing this determinant and solving resulting equation for combination of critical axial compressive load and thermal buckling load, yields

$$N_{x0}^{\wedge}L_{36} = -L_{31}\frac{D_1}{D_3} + L_{32}\frac{D_2}{D_3} + L_{34}\frac{D_4}{D_3} - L_{35}\frac{D_5}{D_3} - L_{33} - K_1L_{37} - K_2L_{38} \tag{33}$$

where D_i $(i = 1, 2, 3, 4, 5)$ are calculated by

$$D_1 = \begin{vmatrix} L_{12} & L_{13} & L_{14} & L_{15} \\ L_{22} & L_{23} & L_{24} & L_{25} \\ L_{42} & L_{43} & L_{44} & L_{45} \\ L_{52} & L_{53} & L_{54} & L_{55} \end{vmatrix}, \quad D_2 = \begin{vmatrix} L_{11} & L_{13} & L_{14} & L_{15} \\ L_{21} & L_{23} & L_{24} & L_{25} \\ L_{41} & L_{43} & L_{44} & L_{45} \\ L_{51} & L_{53} & L_{54} & L_{55} \end{vmatrix}, \quad D_3 = \begin{vmatrix} L_{11} & L_{12} & L_{14} & L_{15} \\ L_{21} & L_{22} & L_{24} & L_{25} \\ L_{41} & L_{42} & L_{44} & L_{45} \\ L_{51} & L_{52} & L_{54} & L_{55} \end{vmatrix},$$

$$D_4 = \begin{vmatrix} L_{11} & L_{12} & L_{13} & L_{15} \\ L_{21} & L_{22} & L_{23} & L_{25} \\ L_{41} & L_{42} & L_{43} & L_{45} \\ L_{51} & L_{52} & L_{53} & L_{55} \end{vmatrix}, \quad D_5 = \begin{vmatrix} L_{11} & L_{12} & L_{13} & L_{14} \\ L_{21} & L_{22} & L_{23} & L_{24} \\ L_{41} & L_{42} & L_{43} & L_{44} \\ L_{51} & L_{52} & L_{53} & L_{54} \end{vmatrix}$$

Equation (33) used to determine the thermal buckling load of stiffened FGM truncated conical shell subjected to thermal load.

Note that the thermal buckling load ΔT contained in $N_{x0}^{\wedge}$ depends on values of m and n, therefore must minimize its expression with respect to m and n, we obtain the critical thermal load ΔT_{cr}.

Uniform temperature rise

Consider a conical shell under uniform temperature rise, namely $\Delta T(z) = \Delta T = \text{const}$. After substituting $\Delta T(z)$ in Eq. (28), and noting expressions of Φ_a, we obtain

(i) First model

Case 1: FGM–Ceramic core–FGM conical shell with FGM stiffener inside

$$N_{x0}^{\wedge} = \Delta T\,(x_0 + L)\,S_1 \tag{34}$$

where

$$S_1 = -\frac{1}{1-\nu}\left[E_{\mathrm{c}}\alpha_{\mathrm{c}}(h-2h_{\mathrm{f}}) + 2h_{\mathrm{f}}\left(E_{\mathrm{m}}\alpha_{\mathrm{m}} + \frac{E_{\mathrm{m}}\alpha_{\mathrm{cm}} + \alpha_{\mathrm{m}}E_{\mathrm{cm}}}{k+1} + \frac{E_{\mathrm{cm}}\alpha_{\mathrm{cm}}}{2k+1}\right)\right]$$

Finally, setting Eq. (40) into Eq. (39), leads to

$$\Delta T = \frac{1}{L_{36}\,(x_0+L)\,S_1}\left(-L_{31}\frac{D_1}{D_3} + L_{32}\frac{D_2}{D_3} + L_{34}\frac{D_4}{D_3} - L_{35}\frac{D_5}{D_3} - L_{33} - K_1L_{37} - K_2L_{38}\right) \tag{35}$$

(ii) Fourth model

Case 5: Ceramic–FGM core–Metal conical shell with FGM stiffener inside

$$N_{x0}^{\wedge} = \Delta T\,(x_0 + L)\,S_2 \tag{36}$$

where

$$S_2 = -\frac{1}{1-\nu}\left[(E_{\mathrm{m}}\alpha_{\mathrm{m}} + E_{\mathrm{c}}\alpha_{\mathrm{c}})\,h_{\mathrm{f}} + \left(E_{\mathrm{m}}\alpha_{\mathrm{m}} + \frac{E_{\mathrm{m}}\alpha_{\mathrm{cm}} + \alpha_{\mathrm{m}}E_{\mathrm{cm}}}{k+1} + \frac{E_{\mathrm{cm}}\alpha_{\mathrm{cm}}}{2k+1}\right)(h-2h_{\mathrm{f}})\right]$$

Finally, setting Eq. (42) into Eq. (39), lead to

$$\Delta T = \frac{1}{L_{36}\,(x_0+L)\,S_2}\left(-L_{31}\frac{D_1}{D_3} + L_{32}\frac{D_2}{D_3} + L_{34}\frac{D_4}{D_3} - L_{35}\frac{D_5}{D_3} - L_{33} - K_1L_{37} - K_2L_{38}\right) \tag{37}$$

Linear temperature distribution through the thickness

If the conical shell is thin enough, a linear temperature distribution across the shell thickness is the first approximation to the solution of the heat conduction equation of the FGM conical shell. Thus, we can assume [5, 42]

$$\Delta T_{(z)} = \Delta T\frac{z}{h} + \frac{T_{\mathrm{a}} + T_{\mathrm{b}}}{2} \tag{38}$$

where T_a and T_b are the temperatures of the internal and external surfaces of conical shell, respectively, and $\Delta T = T_b - T_a$. Substituting Eq. (38) in Eq. (28) by noting expressions of Φ_a, we obtain

(i) First model

Case 1: FGM–Ceramic core–FGM conical shell with FGM stiffener inside

$$N_{x0}^{\wedge} = (x_0 + L)\,\frac{T_a + T_b}{2} S_1 \tag{39}$$

(ii) Fourth model

Case 5: Ceramic–FGM core–Metal conical shell with FGM stiffener inside

$$N_{x0}^{\wedge} = (x_0 + L)\left[\frac{T_a + T_b}{2} S_2 + \Delta T S_3\right] \tag{40}$$

where

$$S_3 = -\frac{1}{(1-\nu)\,h}\left\{\begin{array}{l} \dfrac{E_c\alpha_c - E_m\alpha_m}{2}\left[\left(\dfrac{h}{2}\right)^2 - \left(\dfrac{h}{2} - h_f\right)^2\right] \\ \quad + \left[(E_m\alpha_{cm} + E_{cm}\alpha_m)\left(\dfrac{1}{k+2} - \dfrac{1}{2k+2}\right)\right. \\ \quad \left. + E_{cm}\alpha_{cm}\left(\dfrac{1}{2k+2} - \dfrac{1}{4k+2}\right)\right](h - 2h_f)^2 \end{array}\right\}$$

Substituting $N_{x0}^{\wedge}$ contained in Eqs. (39) and (40) into Eq. (33) and using assumption of Naj et al. [5], $T_b = 0$, we obtain

(i) First model

Case 1: FGM–Ceramic core–FGM conical shell with FGM stiffener inside

$$T_a = \frac{1}{L_{36}M_1}\left(-L_{31}\frac{D_1}{D_3} + L_{32}\frac{D_2}{D_3} + L_{34}\frac{D_4}{D_3} - L_{35}\frac{D_5}{D_3} - L_{33} - K_1L_{37} - K_2L_{38}\right) \tag{41}$$

where

$$M_1 = (x_0 + L)\,\frac{S_1}{2}$$

(ii) Fourth model

Case 5: Ceramic–FGM core–Metal conical shell with FGM stiffener inside

$$T_a = \frac{1}{L_{36}M_2}\left(-L_{31}\frac{D_1}{D_3} + L_{32}\frac{D_2}{D_3} + L_{34}\frac{D_4}{D_3} - L_{35}\frac{D_5}{D_3} - L_{33} - K_1L_{37} - K_2L_{38}\right) \tag{42}$$

where

$$M_2 = (x_0 + L)\left(\frac{S_2}{2} - S_3\right)$$

Mechanical buckling analysis

Consider an ES-FGM truncated conical shell only subjected to the axial compressive mechanical load of intensity $p(N)$ at $x = x_0$ (Figure 3).

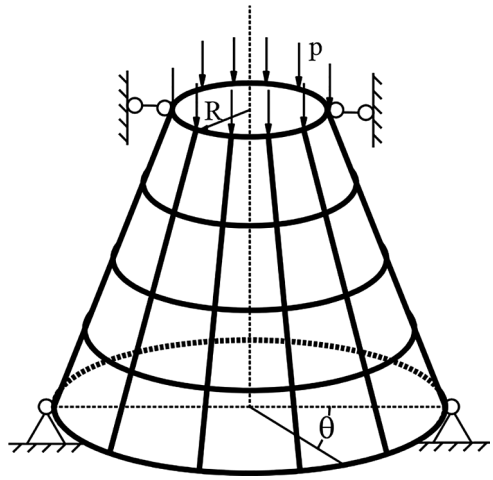

Figure 3. The mechanical buckling of eccentrically stiffened functionally graded materials (ES-FGM).

By the same method as the section above, solving the system (15a)–(15e) with the boundary condition $N_{x0} = -\frac{p}{\cos\beta}$ at $x = x_0$, we obtain

$$N_{x0} = -\frac{px_0}{x\cos\beta}, \quad N_{\theta 0} = 0, \quad N_{x\theta 0} = 0 \tag{43}$$

$$N_{x0}^{\wedge} = xN_{x0} = -\frac{P}{2\pi\,\sin\beta\cos\beta} \tag{44}$$

where $P = 2\pi p x_0 \sin\beta$.

Applying Galerkin method, similarly, by noting $N_{x0}^{\wedge}$ in Eq. (44), we obtain closed-form expression for determining the mechanical buckling load as follows

$$P = -\frac{2\pi\,\sin\beta\cos\beta}{L_{36}}\left(-L_{31}\frac{D_1}{D_3} + L_{32}\frac{D_2}{D_3} + L_{34}\frac{D_4}{D_3} - L_{35}\frac{D_5}{D_3} - L_{33} - K_1L_{37} - K_2L_{38}\right) \tag{45}$$

Minimizing Eq. (45) with respect to m and n, we obtain the critical value of P.

Validation of the present study

To verify the present study, two problems on critical load are compared with results from open literatures.

First comparison

Table 1 using Eq. (45) compares the critical buckling load of unstiffened isotropic truncated conical shell (Stainless steel - SUS304) under axial compressive loads with the results given by Naj et al. [5] and Baruch et al. [61]. The input data base is: $E = 200.10^9$ N/m^2, $k = 0$, $h = 0.01$ m, $R = 100 \times h$, $\nu = 0.3$, $P^* = \frac{P_{\rm cr}}{P_{\rm cl}}$ where $P_{\rm cl} = \frac{2\pi Eh^2\cos^2\alpha}{\sqrt{3(1-\nu^2)}}$ [5] and $P_{\rm cr}$ is found from Eq. (45).

Second comparison

Tables 2 and 3 shows present results compared with those of Naj et al. [5] and Duc et al. [42] for un-stiffened FGM truncated conical shell and the material compositions only vary smoothly along its thickness direction with the power law distribution under uniform thermal load and linear thermal

Table 1. Comparisons of the results on the critical buckling load of unstiffened isotropic truncated conical shells with results of Naj et al. [5] and Baruch et al. [61].

	$L/R = 0.2$			$L/R = 0.5$		
β	Naj et al. [5]	Baruch et al. [61]	P^*(Present)	Naj et al. [5]	Baruch et al. [61]	P^* (Present)
1°	1.005 (7)	1.005 (7)	0.9962(1,6)*	1.0017 (8)	1.002 (8)	0.9979 (3,1)
5°	1.006 (7)	1.006 (7)	0.9962 (1,6)	1.0010 (8)	1.002 (8)	0.9988 (2,8)
10°	1.007 (7)	1.007 (7)	0.9962 (1,6)	1.0000 (8)	1.002 (8)	0.9985 (2,8)
30°	1.0171 (5)	1.017 (5)	0.9980 (1,4)	0.9870 (7)	1.001 (7)	1.0000 (2,7)
60°	1.148 (0)	1.144 (0)	1.1267 (1,1)	1.045 (7)	1.044 (7)	1.0140 (1,7)

*Buckling mode (m, n).

Table 2. Comparisons of the results on the thermal buckling load of unstiffened isotropic truncated conical shells under linear thermal load with results of Naj et al. [5] and Duc et al. [42].

	$\alpha_c \Delta T_{cr}^{\wedge} \times 10^3$					
	$R_1/h = 200$			$R_1/h = 400$		
k	Naj et al. [5]	Duc et al. [42]	Present	Naj et al. [5]	Duc et al. [42]	Present
0	2.75	2.78 (1,17)	2.735 (7,9)*	1.40	1.37 (11,14)	1.369 (9,15)
0.3	2.43	2.44 (1,17)	2.396 (8,5)	1.24	1.20 (11,18)	1.199 (8,17)
1	2.22	2.22 (9,13)	2.135 (8,5)	1.08	1.07 (11,18)	1.068 (8,17)
5	1.92	1.95 (8,1)	1.941 (6,11)	0.99	0.97 (11,13)	0.972 (10,12)
∞	1.75	1.73 (8,8)	1.730 (7,9)	0.89	0.87 (10,25)	0.866 (9,15)

FGM, functionally graded material.
*Buckling mode (m, n).

Table 3. Comparisons of the results on the thermal buckling load of unstiffened isotropic truncated conical shells under linear thermal load with results of Naj et al. [5] and Duc et al. [42].

	$R_1/h = 200$			$R_1/h = 400$		
$\alpha_c \Delta T_{cr}^{\wedge} \times 10^3$	Naj et al. [5]	Duc et al. [42]	Present	Naj et al. [5]	Duc et al. [42]	Present
$T_a = 0$	4.17	4.16 (4,26)	4.1497 (8,5)*	2.08	2.09 (2,27)	2.0762 (8,17)
$T_b = 0$	4.38	4.40 (6,23)	4.3983 (8,5)	2.19	2.20 (10,26)	2.2006 (8,17)

FGM, functionally graded material.
*Buckling mode (m, n).

load, and not resting on elastic foundation, with data base as: $E_m = 200.10^9\ \mathrm{N/m^2}$, $E_c = 380.10^9\ \mathrm{N/m^2}$, $\alpha_m = 11.7 \times 10^{-6} 1/°\mathrm{C}$, $\alpha_c = 7.4 \times 10^{-6} 1/°\mathrm{C}$, $h = 0.01\ \mathrm{m}$, $\nu = 0.3$, $\beta = \frac{\pi}{18}$, $K_1 = 0$, $K_2 = 0$, where $\Delta T_{cr}^{\wedge} = (1 - \nu)\, \Delta T_{cr}$, and ΔT_{cr} is found from Eq. (37) for uniform thermal load case and ΔT_{cr} is found from Eq. (42) for linear thermal load case.

Table 4. Comparisons with results of Dung et al. [41] for FGM sandwich truncated conical shell reinforced by FGM stiffeners.

	β	15°	30°	45°	60°
Case 1	Dung et al. [41]	27.45251 (6,19)*	22.12813 (6,19)	14.78617 (5,18)	7.45014 (4,16)
	Present	26.9185 (6,10)	21.6295 (5,10)	14.4169 (5,9)	7.1698 (4,8)
	Percentage	1.95	2.25	2.50	3.76
Case 2	Dung et al. [41]	28.41658 (8,15)	22.79853 (7,15)	15.22234 (6,14)	7.66136 (5,10)
	Present	27.9788 (7,9)	22.4206 (6,9)	14.8872 (5,9)	7.4018 (4,8)
	Percentage	1.54	1.66	2.20	3.39
Case 3	Dung et al. [41]	21.33585 (5,16)	17.27832 (4,16)	11.57539 (4,15)	5.86457 (3,14)
	Present	20.6411 (4,8)	16.7555 (4,8)	11.1932 (4,8)	5.5457 (3,7)
	%	3.26	3.03	3.30	5.44
Case 4	Dung et al. [41]	22.19521 (7,11)	17.88501 (5,15)	11.97889 (5,11)	6.04788 (4,10)
	Present	21.2933 (2,7)*	17.4869 (5,8)	11.6282 (4,8)	5.7668 (3,7)
	Percentage	4.06	2.23	2.93	4.65

FGM, functionally graded material.
*Buckling mode (m, n).

Third comparison

Table 4 compares present results with those of Dung et al. [41] for FGM sandwich truncated conical shell reinforced by FGM stiffeners, resting on Pasternak elastic foundations, subjected to axial compressive load and the material properties of shells and stiffeners are graded in the thickness direction following a general sigmoid law distribution by analytical method based on the classical shell theory with $E_m = 70.10^9\ \mathrm{N/m^2}$, $E_c = 380.10^9\ \mathrm{N/m^2}$, $\nu = 0.3$, $K_1 = 5 \times 10^5\ \mathrm{N/m^3}$, $K_2 = 3 \times 10^4\ \mathrm{N/m}$, $k_2 = k_3 = k = 1$, $h_f = 0.0015\ \mathrm{m}$, $h_{co} = 0.0025\ \mathrm{m}$, $R = 300 \times h_f$, $L = 2 \times R$, $h_s = 0.003\ \mathrm{m}$, $b_s = 0.002\ \mathrm{m}$, $h_r = 0.003\ \mathrm{m}$, $b_r = 0.002\ \mathrm{m}$, $n_s = 50$, $n_r = 30$, and P_{cr} (MN) is found from Eq. (45).

It is seen from Tables 1–4 that there is a very good agreement between this article results and the results of Naj et al. [5], Baruch et al. [61], Dung et al. [41], and Duc et al. [42].

Numerical results

Effect of stiffener arrangement

Consider an ES-FGM conical shell with input parameters as $E_m = 70.10^9\ \mathrm{N/m^2}$, $E_c = 380.10^9\ \mathrm{N/m^2}$, $\alpha_m = 22.2 \times 10^{-6}1/\mathrm{K}$, $\alpha_c = 5.4 \times 10^{-6}1/\mathrm{K}$, $\nu = 0.3$, $k = 1$, $h = 0.05\ \mathrm{m}$, $R = 2.5\ \mathrm{m}$, $L = 2 \times R$, $\beta = \frac{\pi}{4}$, $K_1 = 2.5 \times 10^7\ \mathrm{N/m^3}$, $K_2 = 2.5 \times 10^5\ \mathrm{N/m}$, $h_s = 0.03\ \mathrm{m}$, $b_s = 0.02\ \mathrm{m}$, $h_r = 0.03\ \mathrm{m}$, $b_r = 0.02\ \mathrm{m}$. Tables 5 and 6, using Eqs. (35), (37), (41), and (42), shows the effect of stiffener on thermal buckling load ΔT_{cr} in two temperature field uniform temperature rise and temperature distribution through the thickness.

As can be seen that stiffener arrangement has significant influence on the critical thermal load of shell. The value of the critical temperature in the case of stiffeners inside smaller than in the case of external stiffeners. Both tables show that, with the same number of stiffeners ($n = 30$), the critical thermal load is greatest for stringer stiffened shell, orthogonally stiffened shell is the second, ring stiffened shell is the third, and the critical load values in the unstiffened case is smaller than stiffened case. In the case of uniform temperature rise, the critical thermal load value is smaller than the case of linear temperature distribution through the thickness.

Effect of stiffener number

With the database of the above section, Tables 7 presents effects of reinforcement stiffener number on critical thermal load ΔT_{cr}. As expected, the obtained results show that the critical thermal load increases when the number of stiffeners increases and inversely. This increase is considerable.

Table 5. Effect of stiffener arrangement on thermal buckling load ΔT_{cr} for Case 1.

	Uniform		Linear temperature distribution ($T_b = 0$)	
ΔT_{cr} (K)	Inside stiffener	Outside stiffener	Inside stiffener	Outside stiffener
Un-stiffened	285.2874 (5,5)*	285.2874 (5,5)	570.5748 (5,5)	570.5748 (5,5)
Stringer ($n_s = 30$)	297.9866 (4,7)	295.8553 (5,4)	595.9732 (4,7)	591.7105 (5,4)
Ring ($n_r = 30$)	287.1580 (5,5)	295.0556 (5,4)	574.3161 (5,5)	590.1113 (5,4)
Orthogonal ($n_s = n_r = 15$)	292.8425 (5,5)	295.5116 (5,4)	585.6850 (5,5)	591.0231 (5,4)

*Buckling mode (m, n).

Table 6. Effect of stiffener arrangement on thermal buckling load ΔT_{cr} for Case 5.

	Uniform		Linear temperature distribution ($T_b = 0$)	
ΔT_{cr} (K)	Inside stiffener	Outside stiffener	Inside stiffener	Outside stiffener
Un-stiffened	225.2755 (5,5)*	225.2755 (5,5)	474.7724 (5,5)	474.7724 (5,5)
Stringer ($n_s = 30$)	242.6644 (4,7)	229.9255 (5,4)	511.4199 (4,7)	484.5725 (5,4)
Ring ($n_r = 30$)	226.8908 (5,5)	232.7340 (6,1)	478.1768 (5,5)	490.4915 (6,1)
Orthogonal ($n_s = n_r = 15$)	235.6625 (5,5)	232.0334 (5,4)	496.6632 (5,5)	489.0149 (5,4)

*Buckling mode (m,n).

Table 7. Effect of stiffener number on critical thermal load ΔT_{cr}.

	ΔT_{cr} (K) (Orthogonal ($n_s = n_r = n/2$), stiffeners at inside)			
	Uniform		Linear temperature distribution ($T_b = 0$)	
Stiffener number (n)	Case 1	Case 5	Case 1	Case 5
10	287.8154 (5,5)*	228.7550 (5,5)	575.6308 (5,5)	479.6058 (5,4)
20	290.3338 (5,5)	232.2173 (5,5)	580.6675 (5,5)	484.3176 (5,4)
30	292.8425 (5,5)	235.6625 (5,5)	585.6850 (5,5)	489.0149 (5,4)
40	295.3417 (5,5)	239.0906 (5,5)	590.6834 (5,5)	493.6978 (5,4)
50	297.8227 (4,7)	242.5019 (5,5)	595.6454 (4,7)	498.3663 (5,4)
60	299.2748 (4,7)	244.9245 (4,7)	598.5496 (4,7)	503.0206 (5,4)

*Buckling mode (m,n).

For example, for Case 1, $\Delta T_{cr} = 287.8154$ K ($n = 10$) for uniform temperature rise in comparison with $\Delta T_{cr} = 299.2748$ K ($n = 60$) increase about 1.04 times; for Case 5, $\Delta T_{cr} = 228.7550$ K ($n = 10$) for uniform temperature rise in comparison with $\Delta T_{cr} = 244.9245$ K ($n = 60$) increase about 1.07 times. The prime reason is that the presence of stiffeners makes the shells become stiffer, so bearing load capacity of them will be better.

Effect of semi-vertex angle β

In this case, the semi-vertex angle β is changed. The effect of semi-vertex angle β on critical thermal load ΔT_{cr} is presented in Table 8. It can be seen that the critical thermal buckling load of sandwich truncated conical shell strongly decreases when semi-vertex angle increases. For example, an orthogonal stiffened shell in Table 8, for Case 1, when the semi-vertex angle varies the values from 5° to 60°, in the case of uniform temperature rise, the critical thermal load ΔT_{cr} decreases from 810.4664 to 195.6100 K, about 75.86% and in the linear temperature distribution, the critical thermal load ΔT_{cr} decreases from 1620.9 to 391.2199 K, about 75.86%.

Table 8. Effect of angle β on critical thermal load ΔT_{cr}.

	ΔT_{cr} (K) (Orthogonal ($n_s = n_r = n/2$), stiffeners at inside)			
	Uniform		Linear temperature distribution ($T_b = 0$)	
β	Case 1	Case 5	Case 1	Case 5
5°	810.4664 (7,6)*	650.6878 (6,6)	1620.9 (7,6)	1336.8 (8,3)
10°	697.4159 (6,7)	558.9150 (6,7)	1394.8 (6,7)	1151.5 (8,2)
20°	535.1976 (6,6)	428.4204 (6,6)	1070.4 (6,6)	887.6080 (7,3)
30°	419.3676 (5,7)	335.8325 (5,7)	838.7353 (5,7)	699.2480 (6,4)
45°	292.8425 (5,5)	235.6625 (5,5)	585.6850 (5,5)	489.0149 (5,4)
60°	195.6100 (4,4)	159.9401 (4,4)	391.2199 (4,4)	330.9807 (5,1)

*Buckling mode (m, n).

Table 9. Effect of core layer on critical thermal load ΔT_{cr}.

	ΔT_{cr} (K)—Uniform; orthogonal (Stiffeners at inside) ($n_s = n_r = 15$)			
h_{co}/h_f	Case 1	Case 3	Case 5	Case 7
0	189.8319 (5,6)*	266.6013 (4,5)	281.3797 (5,6)	274.6792 (5,6)
1	250.6088 (5,5)	265.7473 (4,5)	246.8102 (5,5)	241.5338 (5,6)
2	292.8425 (5,5)	261.6721 (4,4)	235.6625 (5,5)	231.0389 (5,5)
3	323.4413 (5,5)	253.9062 (4,4)	230.3635 (5,5)	226.0274 (5,5)
4	346.4294 (5,5)	247.8966 (4,3)	227.2936 (5,5)	223.1486 (5,5)
5	364.0200 (5,4)	235.4068 (4,3)	225.2932 (5,5)	221.2846 (5,5)

*Buckling mode (m, n).

Table 10. Effect of core layer on critical compression load P_{cr}.

	P_{cr} (MN) Orthogonal (Stiffeners at inside) ($n_s = n_r = 15$)			
h_{co}/h_f	Case 1	Case 3	Case 5	Case 7
0	971.1708 (5,6)*	1363.9 (4,5)	971.7198 (5,6)	948.5801 (5,6)
1	1183.1 (5,5)	1170 (4,5)	989.1143 (5,5)	967.9689 (5,6)
2	1324.6 (5,5)	1087.1 (4,4)	1009.7 (5,5)	989.9281 (5,5)
3	1424.6 (5,5)	1049.7 (4,4)	1025.3 (5,5)	1006 (5,5)
4	1498.5 (5,5)	1029 (4,3)	1036.9 (5,5)	1018 (5,5)
5	1554 (5,4)	1016.8 (4,3)	1045.6 (5,5)	1027 (5,5)

*Buckling mode (m, n).

Effect of core layer h_{co}

With the database of the section before, the influences of the thickness of core layer to coating layer ratio h_{co}/h_f on the critical thermal load ΔT_{cr} and critical compression load P_{cr} are shown in Tables 9 and 10, respectively. It is observed that when h_{co}/h_f increases, ΔT_{cr} and P_{cr} both increase markedly in Cases 1, 5, and 7, but they decrease in Case 3. The critical thermal load and the critical compression load is greatest for Case 1. For example, in Table 9, for Case 1, comparing $\Delta T_{cr} = 189.8319$ K (when $h_{co}/h_f = 0$) with $\Delta T_{cr} = 364.0200$ K (when $h_{co}/h_f = 5$), the critical thermal load increases about 91.76%. For Case 3, comparing $\Delta T_{cr} = 266.6013$ K (when $h_{co}/h_f = 0$) with $\Delta T_{cr} = 235.4068$ K (when $h_{co}/h_f = 5$), the critical thermal load decreases about 11.7%. In Table 10, for Case 1, comparing $P_{cr} = 971.1708$ (MN) (when $h_{co}/h_f = 0$) with $P_{cr} = 1554$ (MN) (when $h_{co}/h_f = 5$), it is observed that the critical load increases about 37.5%, and for Case 3, comparing $P_{cr} = 1363.9$ (MN) (when $h_{co}/h_f = 0$) with $P_{cr} = 1016.8$ (MN) (when $h_{co}/h_f = 5$), the critical load decreases about 25.45%. This result agrees with the actual property of material. As the core layer h_{co} (for Case 1) increases, the volume fraction of ceramic increases, and the value of the critical load is larger. Inversely, for Case 3, when the core layer h_{co} increases, the volume fraction of metal increases, and the value of critical load is smaller.

Effect of the ratio R/h

In this section, the ratio R/h is changed, the other parameters are the same as before. Figures 4 and 5 show effects of the radius-to-thickness ratios R/h on the critical thermal load ΔT_{cr} of shell. We can see that the both critical thermal load ΔT_{cr} decrease markedly with the increase of R/h ratio. These results

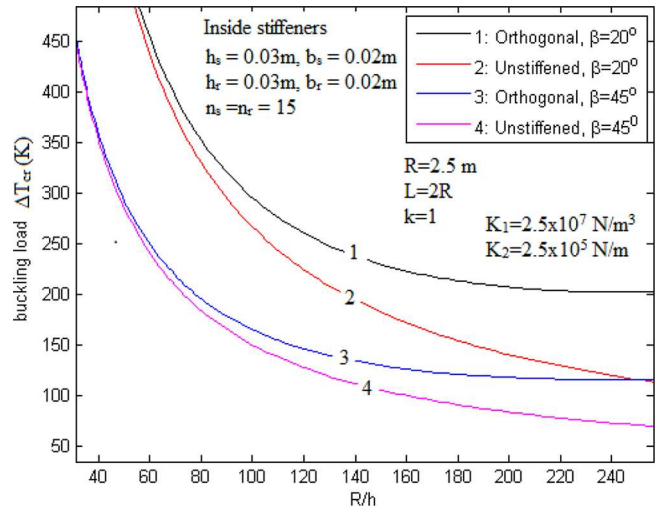

Figure 4. Effects of R/h on critical thermal load ΔT_{cr}—Case 1 (uniform temperature rise).

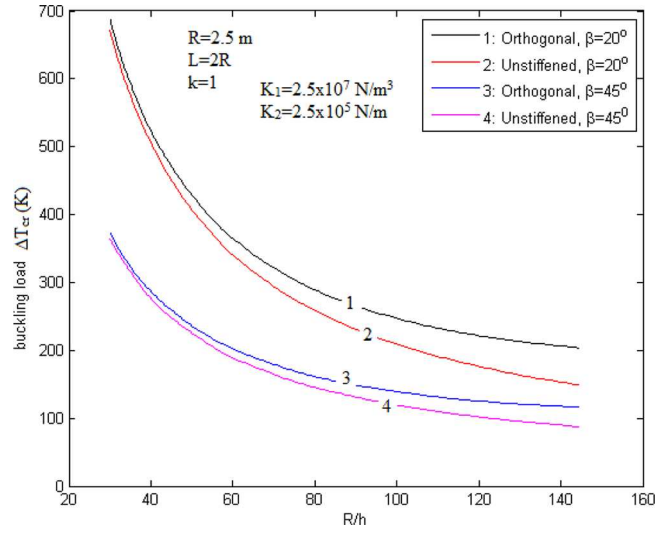

Figure 5. Effects of R/h on critical thermal load ΔT_{cr}—Case 5 (uniform temperature rise).

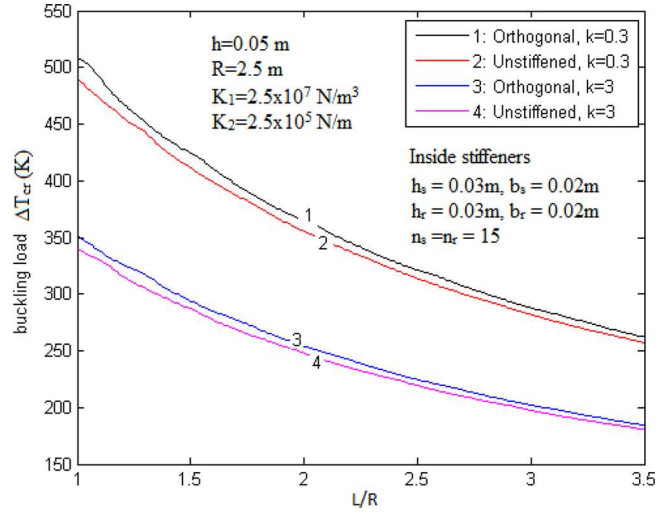

Figure 6. Effects of L/R on critical thermal load ΔT_{cr}—Case 1 (uniform temperature rise).

reflect accurately the actual property of shell because of increasing ratio R/h, h will be reduced, and then the ability of thermal load also will be decreased.

Effect of the ratio L/R

Figures 6 and 7 describe effects of L/R ratio for different volume fraction index (k) on the critical thermal load ΔT_{cr}. It can be observed, the critical thermal load ΔT_{cr} decreases with the increase of length-to-radius ratio L/R. In other words, in the case where R and h are constants, the more the shell length increases, the more the critical thermal load decreases.

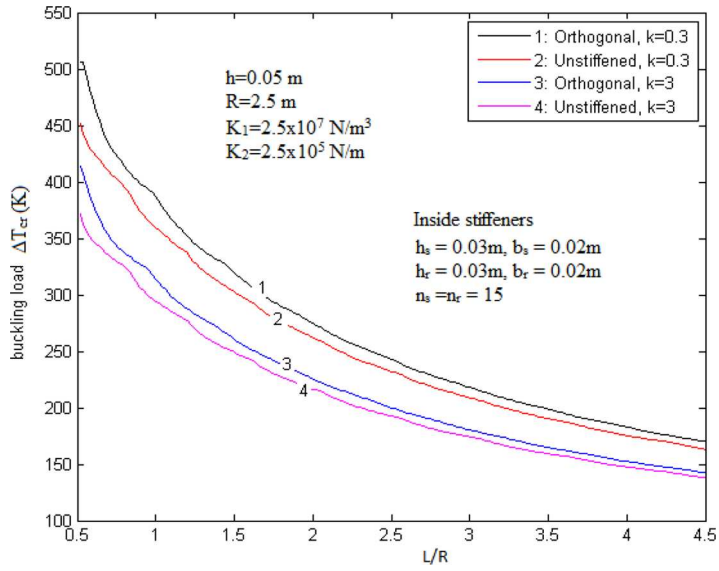

Figure 7. Effects of L/R on critical thermal load ΔT_{cr}—Case 5 (uniform temperature rise).

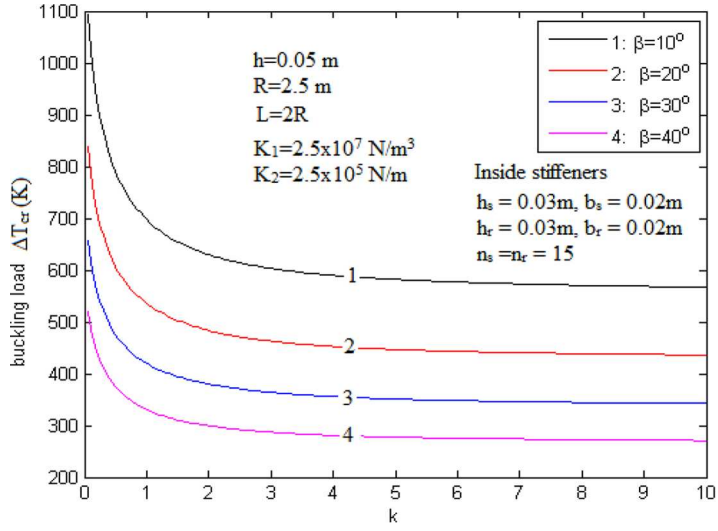

Figure 8. Effects of index volume k on critical thermal load ΔT_{cr}—Case 1 (uniform temperature rise).

Effect of volume fraction index k

The effects of index volume k on critical thermal load ΔT_{cr} for stiffened FGM sandwich truncated conical shell are given by Figures 8 and 9. It is found that the critical thermal load ΔT_{cr} of stiffened FGM truncated conical shell decreases when the value of k increases. This is expected because the elastic modulus E of the ceramic is much larger than of the metal while the volume ratio of ceramic components in the shell decreases with increasing k. Moreover, Figures 8 and 9 also show the relationship curved between the critical thermal load–volume ratio coefficient will be lowered if the semi-vertex angle β increases.

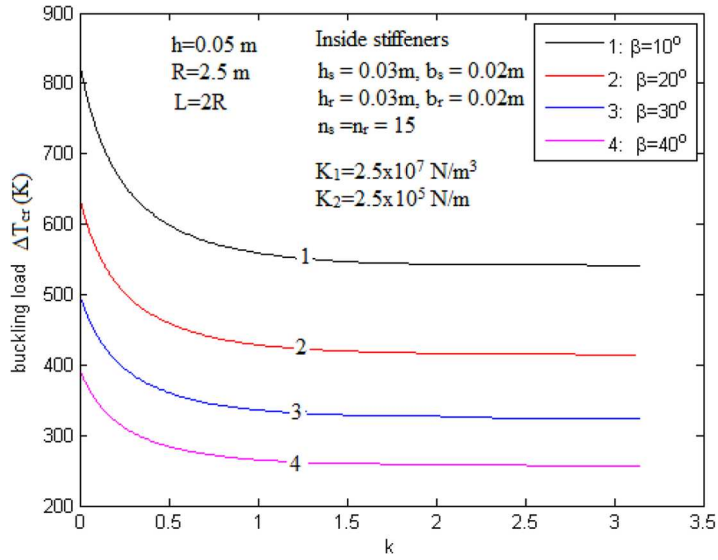

Figure 9. Effects of index volume k on critical thermal load ΔT_{cr}—Case 5 (uniform temperature rise).

Table 11. Effect of elastic foundations on critical thermal load ΔT_{cr}—Case 1 ($n_s = n_r = 15$).

ΔT_{cr} (K) (Uniform, outside stiffener, orthogonal)	$K_2 = 0$ N/m	$K_2 = 10^5$ N/m	$K_2 = 2 \times 10^5$ N/m	$K_2 = 5 \times 10^5$ N/m
$K_1 = 0$ N/m^3	270.9841 (4,7)*	271.6957 (4,7)	272.4072 (4,7)	274.5420 (4,7)
$K_1 = 10^7$ N/m^3	278.4502 (5,5)	279.0076 (5,5)	279.5650 (5,5)	281.2372 (5,5)
$K_1 = 2 \times 10^7$ N/m^3	283.3264 (5,5)	283.8838 (5,5)	284.4412 (5,5)	286.1135 (5,5)
$K_1 = 5 \times 10^7$ N/m^3	297.9550 (5,5)	298.5124 (5,5)	299.0699 (5,5)	300.7421 (5,5)

*Buckling mode (m, n).

Table 12. Effect of elastic foundations on critical thermal load ΔT_{cr}—Case 5 ($n_s = n_r = 15$).

ΔT_{cr} (K) (Uniform, outside orthogonal stiffener)	$K_2 = 0$ N/m	$K_2 = 10^5$ N/m	$K_2 = 2 \times 10^5$ N/m	$K_2 = 5 \times 10^5$ N/m
$K_1 = 0$ N/m^3	216.3770 (4,7)*	217.1282 (4,7)	217.8794 (4,7)	220.1329 (4,7)
$K_1 = 10^7$ N/m^3	224.4066 (4,7)	225.1578 (4,7)	225.9090 (4,7)	228.1625 (4,7)
$K_1 = 2 \times 10^7$ N/m^3	231.6176 (5,5)	232.2060 (5,5)	232.7945 (5,5)	234.5598 (5,5)
$K_1 = 5 \times 10^7$ N/m^3	247.0604 (5,5)	247.6488 (5,5)	248.2373 (5,5)	250.0026 (5,5)

*Buckling mode (m, n).

Effect of elastic foundations on critical thermal load

With the database as the section before, Tables 11 and 12 respectively, show the influence of elastic foundations on the critical thermal load ΔT_{cr} of the ES-FGM sandwich truncated conical shell for Cases 1 and 5. It was found that when increasing the value of the foundation's coefficient K_1 (N/m^3) = (0; 10^7; 2×10^7; 5×10^7) and unchanging the value of the foundation's coefficient K_2 or conversely, increasing the influence of the foundation's coefficient K_2 (N/m) = (0; 10^5; 2×10^5; 5×10^5) and unchanging the coefficient K_1 made the value of the critical thermal load increase. Without elastic foundations ($K_1 = 0, K_2 = 0$), the critical thermal load value is the smallest; and when the foundation's value $K_1 = 5 \times 10^7, K_2 = 5 \times 10^5$ is the largest. For example, in Table 11, for Case 1, the critical thermal load for uniform temperature rise is increased 10.98%.

Effect of axial compressive load on critical thermal load

With the database of the section before, Tables 13 and 14 presents effects of stiffener arrangement and axially pre-loaded P on critical thermal load ΔT_{cr}. It is observed that the value of critical thermal

Table 13. Effect of axially pre-loaded P on critical thermal load ΔT_{cr} (K)—Case 1.

ΔT_{cr}(K) (Inside stiffeners) (m, n)		$P = 0$	$P = 10$ MN	$P = 20$ MN	$P = 30$ MN
Un-stiffened	Uniform	285.2874 (5,5)*	250.5594(5,5)	215.8315 (5,5)	181.1035 (5,5)
	Linear	570.5748 (5,5)	501.1189 (5,5)	431.6629 (5,5)	362.2070 (5,5)
Stringer ($n_s = 30$)	Uniform	297.9866 (4,7)	263.2586 (4,7)	228.5307 (4,7)	193.8027 (4,7)
	Linear	595.9732 (4,7)	526.5173 (4,7)	457.0613 (4,7)	387.6054 (4,7)
Ring ($n_r = 30$)	Uniform	287.1580 (5,5)	252.4301 (5,5)	217.7021 (5,5)	182.9741 (5,5)
	Linear	574.3161 (5,5)	04.8601 (5,5)	435.4042 (5,5)	365.9482 (5,5)
Orthogonal ($n_s = n_r = 15$)	Uniform	292.8425 (5,5)	258.1145 (5,5)	223.3866 (5,5)	188.6586 (5,5)
	Linear	585.6850 (5,5)	516.2291 (5,5)	446.7731 (5,5)	377.3172 (5,5)

*Buckling mode (m, n).

Table 14. Effect of axially pre-loaded P on critical thermal load ΔT_{cr} (K)—Case 5.

ΔT_{cr}(K) (Inside stiffeners) (m, n)		$P = 0$	$P = 10$ MN	$P = 20$ MN	$P = 30$ MN
Un-stiffened	Uniform	225.2755 (5,5)*	188.6147 (5,5)	151.9540 (5,5)	115.2932 (5,5)
	Linear	474.7724 (5,5)	97.5092 (5,5)	320.2459 (5,5)	242.9827 (5,5)
Stringer ($n_s = 30$)	Uniform	242.6644 (4,7)	206.0036 (4,7)	169.3429 (4,7)	132.6821 (4,7)
	Linear	511.4199 (4,7)	434.1567 (4,7)	356.8934 (4,7)	279.6302 (4,7)
Ring ($n_r = 30$)	Uniform	226.8908 (5,5)	190.2301 (5,5)	153.5693 (5,5)	116.9086 (5,5)
	Linear	478.1768 (5,5)	400.9135 (5,5)	323.6503 (5,5)	246.3870 (5,5)
Orthogonal ($n_s = n_r = 15$)	Uniform	235.6625 (5,5)	199.0017 (5,5)	162.3410 (5,5)	125.6802 (5,5)
	Linear	496.6632 (5,5)	19.4000 (5,5)	342.1367 (5,5)	264.8735 (5,5)

*Buckling mode (m, n).

load ΔT_{cr} increases with the decrease of axial preloaded P. This increase is considerable. For example, in Table 13, for Case 1 (uniform temperature rise), comparing $\Delta T_{cr} = 188.6586\,\mathrm{K}$ ($P = 30$) with $\Delta T_{cr} = 292.8425\,\mathrm{K}$ ($P = 0$) in the case of orthogonally stiffener, we can see that the critical thermal load increases about 35.58%.

Effect of elastic foundations on critical axial compressive load

Consider an eccentrically stiffened sandwich truncated conical shells made of FGMs resting on elastic foundations with input parameters as $E_m = 70 \times 10^9\,\mathrm{N/m^2}$, $E_c = 380 \times 10^9\,\mathrm{N/m^2}$, $\nu = 0.3$, $k = 1$, $h = 0.05\,\mathrm{m}$, $R = 50 \times h$, $L = 2 \times R$, $\beta = \frac{\pi}{4}$, $h_s = 0.03\,\mathrm{m}$, $b_s = 0.02\,\mathrm{m}$, $h_r = 0.03\,\mathrm{m}$, $b_r = 0.02\,\mathrm{m}$. Tables 15 and 16, using Eq. (45), shows the effects of elastic foundations on critical compression load P_{cr}. As can be observed, the critical buckling load corresponding to the presence of the both foundation parameters $K_1 = 5 \times 10^7\,\mathrm{N/m^3}$ and $K_2 = 5 \times 10^5\,\mathrm{N/m}$ is the biggest. The critical buckling load of shell without foundation is the smallest. For example, in Table 15 comparing $P_{cr} = 1277.5\,\mathrm{MN}$

Table 15. Effect of elastic foundations on critical compression load P_{cr}—Case 1 ($n_s = n_r = 15$).

P_{cr} (MN) (Outside orthogonal)	$K_2 = 0\,\mathrm{N/m}$	$K_2 = 10^5\,\mathrm{N/m}$	$K_2 = 2 \times 10^5\,\mathrm{N/m}$	$K_2 = 5 \times 10^5\,\mathrm{N/m}$
$K_1 = 0\,\mathrm{N/m^3}$	1239.9 (4,7)*	1243.1 (4,7)	1246.3 (4,7)	1256 (4,7)
$K_1 = 10^7\,\mathrm{N/m^3}$	16005 (1,1)	1277.5 (4,7)	1280.7 (4,7)	1290.4 (4,7)
$K_1 = 2 \times 10^7\,\mathrm{N/m^3}$	16516 (1,1)	16518 (1,1)	16521 (1,1)	16528 (1,1)
$K_1 = 5 \times 10^7\,\mathrm{N/m^3}$	18049 (1,1)	18052 (1,1)	18054 (1,1)	18062 (1,1)

*Buckling mode (m, n).

Table 16. Effect of elastic foundations on critical compression load P_{cr}—Case 5 ($n_s = n_r = 15$).

P_{cr} (MN) (Outside orthogonal)	$K_2 = 0\,\mathrm{N/m}$	$K_2 = 10^5\,\mathrm{N/m}$	$K_2 = 2 \times 10^5\,\mathrm{N/m}$	$K_2 = 5 \times 10^5\,\mathrm{N/m}$
$K_1 = 0\,\mathrm{N/m^3}$	927.1067 (4,7)*	930.3252 (4,7)	933.5438 (4,7)	943.1995 (4,7)
$K_1 = 10^7\,\mathrm{N/m^3}$	961.5109 (4,7)	964.7294 (4,7)	967.9480 (4,7)	977.6037 (4,7)
$K_1 = 2 \times 10^7\,\mathrm{N/m^3}$	992.4076 (4,7)	994.9288 (4,7)	997.4501 (5,5)	1005.00 (5,5)
$K_1 = 5 \times 10^7\,\mathrm{N/m^3}$	1058.6 (5,5)	1061.1 (5,5)	1063.6 (5,5)	1071.2 (5,5)

*Buckling mode (m, n).

($K_1 = 10^7$ N/m^3, $K_2 = 10^5$ N/m) with $P_{cr} = 18062$ MN ($K_1 = 5 \times 10^7$ N/m^3, $K_2 = 5 \times 10^5$ N/m), increases about 14.57 times.

Conclusion

An analytical solution is presented, in this article, to investigate the thermal buckling and mechanical buckling of FGM sandwich truncated conical shells reinforced by FGM stiffeners resting on elastic foundations, subjected to thermal load and axial compressive load. The material properties of shells and stiffeners are assumed to be graded in the thickness direction according to a general sigmoid law distribution and a general power law in terms of the volume fractions of the constituents. The change of spacing between stringers in the meridional direction are taken into account. Four models of coated shell-stiffener arrangements are investigated. Using the adjacent equilibrium criterion, the linearization stability equations in terms of displacement components are established. The couple set of five variable coefficient partial differential equations is investigated by Galerkin. Two cases on uniform temperature rise and linear temperature distribution through the thickness of shell are considered. The closed-form expression for determining the thermal buckling load and critical compression buckling load are obtained. The effects of temperature, foundation, stiffeners, material properties, dimensional parameters and semi-vertex angle on buckling behaviors of shell are considered. The numerical calculations show some remarks as follows:

(i) The critical thermal buckling load (ΔT_{cr}) and the critical axial compressive load (P_{cr}) of FGM sandwich truncated conical shell increase considerably when the thickness of core layer to coating layer $h_{\mathrm{co}}/h_{\mathrm{f}}$ ratio increases in models 1st, 3rd and 4th, and reversely in model 2nd. The critical thermal load and the critical compression load are greatest for model 1.

(ii) The stiffeners, and the volume fraction indices k, k_2, and k_3 strongly affect the critical buckling load. The critical thermal buckling load of FGM sandwich truncated conical shell under both uniform temperature rise and linear temperature distribution across the shell thickness is lower than that of pure ceramic conical shells and higher than the pure metallic conical shells.

(iii) The value of the critical thermal load increases when we increase the stiffener number and inversely. The value of the critical thermal load in case of the uniform temperature rise is smaller than one of the linear temperature distribution through the thickness.

(iv) Critical thermal loads of FGM sandwich truncated conical shells decrease when the axially preloaded P increases.

(v) Critical thermal load of FGM sandwich truncated conical shells decreases when the semi-vertex angle β increases.

(vi) The critical thermal buckling load of FGM sandwich truncated conical shell under both types of thermal loading decreases when R/h increases.

(vii) The critical thermal buckling load of FGM sandwich truncated conical shell under both types of thermal loading decreases when L/R increases.

(viii) Foundation parameters K_1 and K_2 affect strongly on the critical thermal loads and the critical axial compressive load. Furthermore, the foundation coefficient K_1 affects the critical thermal load and the critical axial compressive load more than the foundation coefficient K_2.

Appendix A

$$\lambda_0 = \frac{2\pi sin\beta}{n_{\mathrm{s}}}, \quad d_{\mathrm{s}}(x) = \lambda_0 x, \quad d_{\mathrm{r}} = \frac{L}{n_{\mathrm{r}}}, \quad c_1^0 = \frac{E_{2\mathrm{s}} b_{\mathrm{s}}}{\lambda_0}, \quad c_1(x) = \frac{c_1^0}{x},$$

$$c_2 = \frac{E_{2\mathrm{r}} b_{\mathrm{r}}}{d_{\mathrm{r}}}, \quad A_{11} = A_{22} = \frac{E_1}{1-\nu^2}$$

$$A_{12}=\frac{\nu E_1}{1-\nu^2},\quad A_{44}=A_{55}=\frac{5E_1}{12\,(1+\nu)},\quad A_{66}=\frac{E_1}{2\,(1+\nu)},$$

$$B_{11}=B_{22}=\frac{E_2}{1-\nu^2},\quad B_{12}=\frac{\nu E_2}{1-\nu^2}$$

$$B_{66}=\frac{E_2}{2\,(1+\nu)},\quad D_{11}=D_{22}=\frac{E_3}{1-\nu^2},\quad D_{12}=\frac{\nu E_3}{1-\nu^2},\quad D_{66}=\frac{E_3}{2\,(1+\nu)}$$

$$\Phi_{\mathrm{a}}=-\int_{-\frac{h}{2}}^{\frac{h}{2}}\frac{E_{\mathrm{sh}}\alpha_{\mathrm{sh}}\Delta T(z)}{1-\nu}\mathrm{d}z,\Phi_{\mathrm{b}}=-\int_{-\frac{h}{2}}^{\frac{h}{2}}\frac{E_{\mathrm{sh}}\alpha_{\mathrm{sh}}\Delta T(z)z}{1-\nu}\mathrm{d}z$$

(i) For the first model (FGM–Ceramic core–FGM conical shell)

$$E_{\mathrm{sh}}=\begin{cases}E_{\mathrm{c}}+E_{\mathrm{mc}}\left(\dfrac{z-z_1}{z_2-z_1}\right)^k, & z_1\le z\le z_2,\\ E_{\mathrm{m}}, \quad z_2\le z\le z_3,\\ E_{\mathrm{c}}+E_{\mathrm{mc}}\left(\dfrac{z-z_4}{z_3-z_4}\right)^k, & z_3\le z\le z_4,\end{cases},\quad \alpha_{\mathrm{sh}}=\begin{cases}\alpha_{\mathrm{c}}+\alpha_{\mathrm{mc}}\left(\dfrac{z-z_1}{z_2-z_1}\right)^k, & z_1\le z\le z_2\\ \alpha_{\mathrm{m}}, z_2\le z\le z_3\\ \alpha_{\mathrm{c}}+\alpha_{\mathrm{mc}}\left(\dfrac{z-z_4}{z_3-z_4}\right)^k, & z_3\le z\le z_4\end{cases}$$

$$E_1=E_{\mathrm{m}}h+E_{\mathrm{cm}}\left[\frac{z_2-z_1}{k+1}+z_3-z_2-\frac{z_3-z_4}{k+1}\right],\ E_2=0$$

$$E_3=\frac{E_{\mathrm{m}}h^3}{12}+E_{\mathrm{cm}}\left[\begin{array}{l}\dfrac{(z_2-z_1)^3}{k+3}+\dfrac{2z_1\,(z_2-z_1)^2}{k+2}+\dfrac{z_1^2\,(z_2-z_1)}{k+1}+\dfrac{z_3^3-z_2^3}{3}\\ -\dfrac{(z_3-z_4)^3}{k+3}-\dfrac{2z_4\,(z_3-z_4)^2}{k+2}-\dfrac{z_4^2\,(z_3-z_4)}{k+1}\end{array}\right]$$

Case 1, stiffeners at inside:

$$E_{\mathrm{s}}=E_{\mathrm{m}}+E_{\mathrm{cm}}\left(\frac{z_1-z}{h_{\mathrm{s}}}\right)^{k_2},\quad -\frac{h}{2}-h_{\mathrm{s}}\le z\le -\frac{h}{2};$$

$$E_{\mathrm{r}}=E_{\mathrm{m}}+E_{\mathrm{cm}}\left(\frac{z_1-z}{h_r}\right)^{k_3},\quad -\frac{h}{2}-h_{\mathrm{r}}\le z\le -\frac{h}{2}$$

$$E_{1\mathrm{s}}=E_{\mathrm{m}}h_{\mathrm{s}}+E_{\mathrm{cm}}\frac{h_{\mathrm{s}}}{k_2+1},\quad E_{2\mathrm{s}}=\frac{E_{\mathrm{m}}}{2}\left[z_1^2-(z_1-h_{\mathrm{s}})^2\right]+E_{\mathrm{cm}}\left[\frac{z_1h_{\mathrm{s}}}{k_2+1}-\frac{h_{\mathrm{s}}^2}{k_2+2}\right]$$

$$E_{3\mathrm{s}}=\frac{E_{\mathrm{m}}}{3}\left[z_1^3-(z_1-h_{\mathrm{s}})^3\right]+E_{\mathrm{cm}}\left[\frac{h_{\mathrm{s}}^3}{k_2+3}-\frac{2z_1h_{\mathrm{s}}^2}{k_2+2}+\frac{z_1^2h_{\mathrm{s}}}{k_2+1}\right]$$

$$E_{1\mathrm{r}}=E_{\mathrm{m}}h_{\mathrm{r}}+E_{\mathrm{cm}}\frac{h_{\mathrm{r}}}{k_3+1},\quad E_{2\mathrm{r}}=\frac{E_{\mathrm{m}}}{2}\left[z_1^2-(z_1-h_{\mathrm{r}})^2\right]+E_{\mathrm{cm}}\left[\frac{z_1h_{\mathrm{r}}}{k_3+1}-\frac{h_{\mathrm{r}}^2}{k_3+2}\right]$$

$$E_{3\mathrm{r}}=\frac{E_{\mathrm{m}}}{3}\left[z_1^3-(z_1-h_{\mathrm{r}})^3\right]+E_{\mathrm{cm}}\left[\frac{h_{\mathrm{r}}^3}{k_3+3}-\frac{2z_1h_{\mathrm{r}}^2}{k_3+2}+\frac{z_1^2h_{\mathrm{r}}}{k_3+1}\right]$$

Case 2, stiffeners at outside:

$$E_s = E_m + E_{cm}\left(\frac{z - z_4}{h_s}\right)^{k_2}, \frac{h}{2} \le z \le \frac{h}{2} + h_s;$$

$$E_r = E_m + E_{cm}\left(\frac{z - z_4}{h_r}\right)^{k_3}, \frac{h}{2} \le z \le \frac{h}{2} + h_r$$

$$E_{1s} = E_m h_s + E_{cm}\frac{h_s}{k_2 + 1}, \quad E_{2s} = \frac{E_m}{2}\left[(z_4 + h_s)^2 - z_4^2 -\right] + E_{cm}\left[\frac{z_4 h_s}{k_2 + 1} + \frac{h_s^2}{k_2 + 2}\right]$$

$$E_{3s} = \frac{E_m}{3}\left[(z_4 + h_s)^3 - z_4^3\right] + E_{cm}\left[\frac{h_s^3}{k_2 + 3} + \frac{2z_4 h_s^2}{k_2 + 2} + \frac{z_4^2 h_s}{k_2 + 1}\right]$$

$$E_{1r} = E_m h_r + E_{cm}\frac{h_r}{k_3 + 1}, \quad E_{2r} = \frac{E_m}{2}\left[(z_4 + h_r)^2 - z_4^2 -\right] + E_{cm}\left[\frac{z_4 h_r}{k_3 + 1} + \frac{h_r^2}{k_3 + 2}\right]$$

$$E_{3s} = \frac{E_m}{3}\left[(z_4 + h_r)^3 - z_4^3\right] + E_{cm}\left[\frac{h_r^3}{k_3 + 3} + \frac{2z_4 h_r^2}{k_3 + 2} + \frac{z_4^2 h_r}{k_3 + 1}\right]$$

(ii) For the second model (FGM–Metal core–FGM conical shell)

$$E_{sh} = \begin{cases} E_c + E_{mc}\left(\dfrac{z - z_1}{z_2 - z_1}\right)^k, & z_1 \le z \le z_2, \\ E_m, \quad z_2 \le z \le z_3, \\ E_c + E_{mc}\left(\dfrac{z - z_4}{z_3 - z_4}\right)^k, & z_3 \le z \le z_4, \end{cases} \quad ; \quad \alpha_{sh} = \begin{cases} \alpha_c + \alpha_{mc}\left(\dfrac{z - z_1}{z_2 - z_1}\right)^k, z_1 \le z \le z_2 \\ \alpha_m, \quad z_2 \le z \le z_3 \\ \alpha_c + \alpha_{mc}\left(\dfrac{z - z_4}{z_3 - z_4}\right)^k, z_3 \le z \le z_4 \end{cases}$$

$$E_1 = E_c h + E_{mc}\left[\frac{z_2 - z_1}{k + 1} + z_3 - z_2 - \frac{z_3 - z_4}{k + 1}\right], E_2 = 0$$

$$E_3 = \frac{E_c h^3}{12} + E_{mc}\left[\begin{array}{l} \dfrac{(z_2 - z_1)^3}{k + 3} + \dfrac{2z_1 (z_2 - z_1)^2}{k + 2} + \dfrac{z_1^2 (z_2 - z_1)}{k + 1} + \dfrac{z_3^3 - z_2^3}{3} \\ -\dfrac{(z_3 - z_4)^3}{k + 3} - \dfrac{2z_4 (z_3 - z_4)^2}{k + 2} - \dfrac{z_4^2 (z_3 - z_4)}{k + 1} \end{array}\right]$$

Case 3, stiffeners at inside:

$$E_s = E_c + E_{mc}\left(\frac{z_1 - z}{h_s}\right)^{k_2}, \quad -\frac{h}{2} - h_s \le z \le -\frac{h}{2};$$

$$E_r = E_c + E_{mc}\left(\frac{z_1 - z}{h_r}\right)^{k_3}, \quad -\frac{h}{2} - h_r \le z \le -\frac{h}{2}$$

$$E_{1s} = E_c h_s + E_{mc}\frac{h_s}{k_2 + 1}, \quad E_{2s} = \frac{E_c}{2}\left[z_1^2 - (z_1 - h_s)^2\right] + E_{mc}\left[\frac{z_1 h_s}{k_2 + 1} - \frac{h_s^2}{k_2 + 2}\right]$$

$$E_{3s} = \frac{E_c}{3}\left[z_1^3 - (z_1 - h_s)^3\right] + E_{mc}\left[\frac{h_s^3}{k_2 + 3} - \frac{2z_1 h_s^2}{k_2 + 2} + \frac{z_1^2 h_s}{k_2 + 1}\right]$$

$$E_{1r} = E_c h_r + E_{mc}\frac{h_r}{k_3+1}, \quad E_{2r} = \frac{E_c}{2}\left[z_1^2 - (z_1 - h_r)^2\right] + E_{mc}\left[\frac{z_1 h_r}{k_3+1} - \frac{h_r^2}{k_3+2}\right]$$

$$E_{3r} = \frac{E_c}{3}\left[z_1^3 - (z_1 - h_r)^3\right] + E_{mc}\left[\frac{h_r^3}{k_3+3} - \frac{2z_1 h_r^2}{k_3+2} + \frac{z_1^2 h_r}{k_3+1}\right]$$

Case 4, stiffeners at outside:

$$E_s = E_c + E_{mc}\left(\frac{z-z_4}{h_s}\right)^{k_2}, \frac{h}{2} \le z \le \frac{h}{2} + h_s; \quad E_r = E_c + E_{mc}\left(\frac{z-z_4}{h_r}\right)^{k_3}, \frac{h}{2} \le z \le \frac{h}{2} + h_r$$

$$E_{1s} = E_c h_s + E_{mc}\frac{h_s}{k_2+1}, \quad E_{2s} = \frac{E_c}{2}\left[(z_4+h_s)^2 - z_4^2 -\right] + E_{mc}\left[\frac{z_4 h_s}{k_2+1} + \frac{h_s^2}{k_2+2}\right]$$

$$E_{3s} = \frac{E_c}{3}\left[(z_4+h_s)^3 - z_4^3\right] + E_{mc}\left[\frac{h_s^3}{k_2+3} + \frac{2z_4 h_s^2}{k_2+2} + \frac{z_4^2 h_s}{k_2+1}\right]$$

$$E_{1r} = E_c h_r + E_{mc}\frac{h_r}{k_3+1}, \quad E_{2r} = \frac{E_c}{2}\left[(z_4+h_r)^2 - z_4^2 -\right] + E_{mc}\left[\frac{z_4 h_r}{k_3+1} + \frac{h_r^2}{k_3+2}\right]$$

$$E_{3s} = \frac{E_c}{3}\left[(z_4+h_r)^3 - z_4^3\right] + E_{mc}\left[\frac{h_r^3}{k_3+3} + \frac{2z_4 h_r^2}{k_3+2} + \frac{z_4^2 h_r}{k_3+1}\right]$$

(iii) For the third model (Ceramic–FGM core–Metal conical shell)

$$E_{sh} = \begin{cases} E_m, & z_1 \le z \le z_2, \\ E_m + E_{cm}\left(\dfrac{z-z_2}{z_3-z_2}\right)^k, & z_2 \le z \le z_3 \\ E_c, & z_3 \le z \le z_4, \end{cases}; \quad \alpha_{sh} = \begin{cases} \alpha_m, & z_1 \le z \le z_2 \\ \alpha_m + \alpha_{cm}\left(\dfrac{z-z_2}{z_3-z_2}\right)^k, & z_2 \le z \le z_3 \\ \alpha_c, & z_3 \le z \le z_4 \end{cases}$$

$$E_1 = E_m h + E_{cm}\left[\frac{z_3-z_2}{k+1} + z_4 - z_3\right], \quad E_2 = E_{cm}\left[\frac{(z_3-z_2)^2}{k+2} + \frac{z_2(z_3-z_2)}{k+1} + \frac{z_4^2 - z_3^2}{2}\right]$$

$$E_3 = \frac{E_m h^3}{12} + E_{cm}\left[\frac{(z_3-z_2)^3}{k+3} + \frac{2z_2(z_3-z_2)^2}{k+2} + \frac{z_2^2(z_3-z_2)}{k+1} + \frac{z_4^3 - z_3^3}{3}\right]$$

Case 5, stiffeners at inside: the E_{is}, E_{ir} $(i = 1 \div 3)$ are the same as the first model.
Case 6, stiffeners at outside: the E_{is}, E_{ir} $(i = 1 \div 3)$ are the same as the second model.

(iv) For the fourth model (Metal–FGM core–Ceramic conical shell)

$$E_{sh} = \begin{cases} E_c, & z_1 \le z \le z_2, \\ E_c + E_{mc}\left(\dfrac{z-z_2}{z_3-z_2}\right)^k, & z_2 \le z \le z_3 \\ E_m, & z_3 \le z \le z_4, \end{cases}; \quad \alpha_{sh} = \begin{cases} \alpha_c, & z_1 \le z \le z_2 \\ \alpha_c + \alpha_{mc}\left(\dfrac{z-z_2}{z_3-z_2}\right)^k, & z_2 \le z \le z_3 \\ \alpha_m, & z_3 \le z \le z_4 \end{cases}$$

$$E_1 = E_c h + E_{mc}\left[\frac{z_3-z_2}{k+1} + z_4 - z_3\right], \quad E_2 = E_{mc}\left[\frac{(z_3-z_2)^2}{k+2} + \frac{z_2(z_3-z_2)}{k+1} + \frac{z_4^2 - z_3^2}{2}\right]$$

$$E_3 = \frac{E_c h^3}{12} + E_{mc}\left[\frac{(z_3-z_2)^3}{k+3} + \frac{2z_2(z_3-z_2)^2}{k+2} + \frac{z_2^2(z_3-z_2)}{k+1} + \frac{z_4^3 - z_3^3}{3}\right]$$

Case 7, stiffeners at inside, the E_{is}, E_{ir} $(i = 1 \div 3)$ are the same as the second model.

Case 8, stiffeners at outside, the E_{is}, E_{ir} $(i = 1 \div 3)$ are the same as in model 1.

$$E_{mc} = E_m - E_c, \quad E_{cm} = E_c - E_m, \quad \alpha_{mc} = \alpha_m - \alpha_c, \quad \alpha_{cm} = \alpha_c - \alpha_m$$

Appendix B

In Eqs. (27)–(31):

$$S_{11} = \left[A_{11}x + \frac{E_{1s}b_s}{\lambda_0}\right]\frac{\partial^2}{\partial x^2} + \frac{1}{x\sin^2\beta}A_{66}\frac{\partial^2}{\partial\theta^2} + A_{11}\frac{\partial}{\partial x} - \left[A_{22} + \frac{E_{1r}b_r}{d_r}\right]\frac{1}{x}$$

$$S_{12} = \frac{1}{\sin\beta}(A_{12} + A_{66})\frac{\partial^2}{\partial x\partial\theta} - \frac{1}{x\sin\beta}\left[A_{22} + A_{66} + \frac{E_{1r}b_r}{d_r}\right]\frac{\partial}{\partial\theta}$$

$$S_{13} = \cot\beta A_{12}\frac{\partial}{\partial x} - \cot\beta\frac{1}{x}\left[A_{22} + \frac{E_{1r}b_r}{d_r}\right]$$

$$S_{14} = \left(B_{11}x + c_1^0\right)\frac{\partial^2}{\partial x^2} + \frac{1}{x\sin^2\beta}B_{66}\frac{\partial^2}{\partial\theta^2} + B_{11}\frac{\partial}{\partial x} - (B_{22} + c_2)\frac{1}{x}$$

$$S_{15} = \frac{1}{\sin\beta}(B_{12} + B_{66})\frac{\partial^2}{\partial x\partial\theta} - \frac{1}{x\sin\beta}(B_{22} + B_{66} + c_2)\frac{\partial}{\partial\theta}$$

$$S_{21} = \frac{1}{\sin\beta}(A_{12} + A_{66})\frac{\partial^2}{\partial x\partial\theta} + \frac{1}{x\sin\beta}\left[A_{22} + A_{66} + \frac{E_{1r}b_r}{d_r}\right]\frac{\partial}{\partial\theta}$$

$$S_{22} = A_{66}x\frac{\partial^2}{\partial x^2} + \frac{1}{x\sin^2\beta}\left[A_{22} + \frac{E_{1r}b_r}{d_r}\right]\frac{\partial^2}{\partial\theta^2} + A_{66}\frac{\partial}{\partial x} - A_{66}\frac{1}{x}$$

$$S_{23} = \left(A_{22} + \frac{E_{1r}b_r}{d_r}\right)\cot\beta\frac{1}{x\sin\beta}\frac{\partial}{\partial\theta}$$

$$S_{24} = \frac{1}{\sin\beta}(B_{12} + B_{66})\frac{\partial^2}{\partial x\partial\theta} + \frac{1}{x\sin\beta}(B_{22} + B_{66} + c_2)\frac{\partial}{\partial\theta}$$

$$S_{25} = B_{66}x\frac{\partial^2}{\partial x^2} + \frac{1}{x\sin^2\beta}(B_{22} + c_2)\frac{\partial^2}{\partial\theta^2} + B_{66}\frac{\partial}{\partial x} - B_{66}\frac{1}{x}$$

$$S_{31} = \left(B_{11}x + c_1^0\right)\frac{\partial^3}{\partial x^3} + \frac{1}{x\sin^2\beta}(B_{12} + 2B_{66})\frac{\partial^3}{\partial x\partial\theta^2} + 2B_{11}\frac{\partial^2}{\partial x^2}$$
$$+ \frac{1}{x^2\sin^2\beta}(B_{22} + c_2)\frac{\partial^2}{\partial\theta^2} - \left[A_{12}\cot\beta + (B_{22} + c_2)\frac{1}{x}\right]\frac{\partial}{\partial x}$$
$$- \left\{\left[A_{22} + \frac{E_{1r}b_r}{d_r}\right]\cot\beta - (B_{22} + c_2)\frac{1}{x}\right\}\frac{1}{x}$$

$$S_{32} = (B_{12} + 2B_{66})\frac{1}{\sin\beta}\frac{\partial^3}{\partial x^2\partial\theta} + (B_{22} + c_2)\frac{1}{x^2\sin^3\beta}\frac{\partial^3}{\partial\theta^3} - (B_{22} + c_2)\frac{1}{x\sin\beta}\frac{\partial^2}{\partial x\partial\theta}$$
$$- \left\{\left[A_{22} + \frac{E_{1r}b_r}{d_r}\right]\cot\beta - (B_{22} + c_2)\frac{1}{x}\right\}\frac{1}{x\sin\beta}\frac{\partial}{\partial\theta}$$

$$S_{33} = B_{12}\cot\beta\frac{\partial^2}{\partial x^2} + (B_{22}+c_2)\cot\beta\frac{1}{x^2\sin^2\beta}\frac{\partial^2}{\partial\theta^2} - (B_{22}+c_2)\cot\beta\frac{1}{x}\frac{\partial}{\partial x}$$
$$- \left\{\left[A_{22} + \frac{E_{1r}b_r}{d_r}\right]\cot\beta - (B_{22}+c_2)\frac{1}{x}\right\}\cot\beta\frac{1}{x}$$

$$S_{34} = \left[D_{11}x + \frac{E_{3s}b_s}{\lambda_0}\right]\frac{\partial^3}{\partial x^3} + \frac{1}{x\sin^2\beta}(D_{12}+2D_{66})\frac{\partial^3}{\partial x\partial\theta^2} + 2D_{11}\frac{\partial^2}{\partial x^2}$$
$$+ \left[D_{22} + \frac{E_{3r}b_r}{d_r}\right]\frac{1}{x^2\sin^2\beta}\frac{\partial^2}{\partial\theta^2} - \left[B_{12}\cot\beta + \left(D_{22} + \frac{E_{3r}b_r}{d_r}\right)\frac{1}{x}\right]\frac{\partial}{\partial x}$$
$$- \left\{(B_{22}+c_2)\cot\beta - \left[D_{22} + \frac{E_{3r}b_r}{d_r}\right]\frac{1}{x}\right\}\frac{1}{x}$$

$$S_{35} = (D_{12}+2D_{66})\frac{1}{\sin\beta}\frac{\partial^3}{\partial x^2\partial\theta} + \left[D_{22} + \frac{E_{3r}b_r}{d_r}\right]\frac{1}{x^2\sin^3\beta}\frac{\partial^3}{\partial\theta^3}$$
$$- \left[D_{22} + \frac{E_{3r}b_r}{d_r}\right]\frac{1}{x\sin\beta}\frac{\partial^2}{\partial x\partial\theta} - \left[(B_{22}+c_2)\cot\beta - \left(D_{22} + \frac{E_{3r}b_r}{d_r}\right)\frac{1}{x}\right]\frac{1}{x\sin\beta}\frac{\partial}{\partial\theta}$$

$$S_{36} = \frac{\partial^2}{\partial x^2}, \quad S_{37} = -x, \quad S_{38} = x\frac{\partial^2}{\partial x^2} + \frac{1}{x\sin^2\beta}\frac{\partial^2}{\partial\theta^2} + \frac{\partial}{\partial x}$$

$$S_{41} = \left(B_{11}x + c_1^0\right)\sin\beta\frac{\partial^2}{\partial x^2} + B_{66}\frac{1}{x\sin\beta}\frac{\partial^2}{\partial\theta^2} + B_{11}\sin\beta\frac{\partial}{\partial x} - (B_{22}+c_2)\sin\beta\frac{1}{x}$$

$$S_{42} = (B_{12}+B_{66})\frac{\partial^2}{\partial x\partial\theta} - (B_{22}+B_{66}+c_2)\frac{1}{x}\frac{\partial}{\partial\theta}$$

$$S_{43} = (B_{12}\cos\beta - A_{44}x\sin\beta)\frac{\partial}{\partial x} - (B_{22}+c_2)\cos\beta\frac{1}{x}$$

$$S_{44} = \left[D_{11}x + \frac{E_{3s}b_s}{\lambda_0}\right]\sin\beta\frac{\partial^2}{\partial x^2} + \frac{1}{x\sin\beta}D_{66}\frac{\partial^2}{\partial\theta^2} + D_{11}\sin\beta\frac{\partial}{\partial x} - \left\{A_{44}x + \left[D_{22} + \frac{E_{3r}b_r}{d_r}\right]\frac{1}{x}\right\}\sin\beta$$

$$S_{45} = (D_{12}+D_{66})\frac{\partial^2}{\partial x\partial\theta} - \left[D_{22} + D_{66} + \frac{E_{3r}b_r}{d_r}\right]\frac{1}{x}\frac{\partial}{\partial\theta}$$

$$S_{51} = (B_{12}+B_{66})\frac{\partial^2}{\partial x\partial\theta} + (B_{22}+B_{66}+c_2)\frac{1}{x}\frac{\partial}{\partial\theta}$$

$$S_{52} = B_{66}x\sin\beta\frac{\partial^2}{\partial x^2} + \frac{1}{x\sin\beta}(B_{22}+c_2)\frac{\partial^2}{\partial\theta^2} + B_{66}\sin\beta\frac{\partial}{\partial x} - B_{66}\sin\beta\frac{1}{x}$$

$$S_{53} = -\left[A_{55} - (B_{22}+c_2)\cot\beta\frac{1}{x}\right]\frac{\partial}{\partial\theta}$$

$$S_{54} = (D_{12}+D_{66})\frac{\partial^2}{\partial x\partial\theta} + \left[D_{22} + D_{66} + \frac{E_{3r}b_r}{d_r}\right]\frac{1}{x}\frac{\partial}{\partial\theta}$$

$$S_{55} = D_{66}x\sin\beta\frac{\partial^2}{\partial x^2} + \left[D_{22} + \frac{E_{3r}b_r}{d_r}\right]\frac{1}{x\sin\beta}\frac{\partial^2}{\partial\theta^2} + D_{66}\sin\beta\frac{\partial}{\partial x} - \left[A_{55}x + D_{66}\frac{1}{x}\right]\sin\beta$$

Appendix C

In Eqs. (32a)–(32e):

$$L_{11} = -\frac{m^2\pi^3}{L^2}A_{11}\sin\beta\left[\frac{(x_0+L)^4 - x_0^4}{8} + \frac{3L^3\,(2x_0+L)}{8m^2\pi^2}\right]$$

$$-\frac{\pi}{4}L\,(2x_0+L)\sin\beta\left[A_{22} + \frac{n^2}{\sin^2\beta}A_{66} + \frac{E_{1r}b_r}{d_r}\right]$$

$$-\frac{m^2\pi^3}{L^2}\frac{E_{1s}b_s}{\lambda_0}\sin\beta\left[\frac{(x_0+L)^3 - x_0^3}{6} + \frac{L^3}{4m^2\pi^2}\right] + \frac{\pi}{4}L\,(2x_0+L)\,A_{11}\sin\beta$$

$$L_{12} = -\frac{mn\pi^2}{L}\,(A_{12}+A_{66})\left[\frac{(x_0+L)^3 - x_0^3}{6} + \frac{L^3}{4m^2\pi^2}\right] - \frac{nL^2}{4m}\left[A_{22} + A_{66} + \frac{E_{1r}b_r}{d_r}\right]$$

$$L_{13} = \frac{m\pi^2}{L}\cot\beta\sin\beta A_{12}\left[\frac{(x_0+L)^3 - x_0^3}{6} + \frac{L^3}{4m^2\pi^2}\right] + \cot\beta\sin\beta\frac{L^2}{4m}\left[A_{22} + \frac{E_{1r}b_r}{d_r}\right]$$

$$L_{14} = -\frac{m^2\pi^3}{L^2}B_{11}\sin\beta\left[\frac{(x_0+L)^4 - x_0^4}{8} + \frac{3L^3\,(2x_0+L)}{8m^2\pi^2}\right]$$

$$-\frac{\pi}{4}L\,(2x_0+L)\sin\beta(B_{22} + \frac{n^2}{\sin^2\beta}B_{66} + c_2)$$

$$-\frac{m^2\pi^3}{L^2}c_1^0\sin\beta\left[\frac{(x_0+L)^3 - x_0^3}{6} + \frac{L^3}{4m^2\pi^2}\right] + \frac{\pi}{4}L\,(2x_0+L)\,B_{11}\sin\beta$$

$$L_{15} = -\frac{mn\pi^2}{4}\frac{1}{\sin\beta}\,(2x_0+L)\,(B_{12}+B_{66})$$

$$L_{21} = -\frac{mn\pi^2}{L}\,(A_{12}+A_{66})\left[\frac{(x_0+L)^3 - x_0^3}{6} - \frac{L^3}{4m^2\pi^2}\right] - \frac{nL^2}{4m}\left[A_{22} + A_{66} + \frac{E_{1r}b_r}{d_r}\right]$$

$$L_{22} = -\frac{m^2\pi^3}{L^2}A_{66}\sin\beta\left[\frac{(x_0+L)^4 - x_0^4}{8} - \frac{3L^3\,(2x_0+L)}{8m^2\pi^2}\right] - \frac{\pi}{4}L\,(2x_0+L)\,A_{66}\sin\beta$$

$$-\frac{\pi}{4}L\,(2x_0+L)\sin\beta\left\{\frac{n^2}{\sin^2\beta}\left[A_{22} + \frac{E_{1r}b_r}{d_r}\right] + A_{66}\right\}$$

$$L_{23} = \frac{n\pi}{4}L\,(2x_0+L)\cot\beta\left[A_{22} + \frac{E_{1r}b_r}{d_r}\right]$$

$$L_{24} = -\frac{mn\pi^2}{L}\,(B_{12}+B_{66})\left[\frac{(x_0+L)^3 - x_0^3}{6} - \frac{L^3}{4m^2\pi^2}\right] - \frac{nL^2}{4m}\,(B_{22}+B_{66}+c_2)$$

$$L_{25} = -\frac{m^2\pi^3}{L^2}B_{66}\left[\frac{(x_0+L)^3 - x_0^3}{6} - \frac{L^3}{4m^2\pi^2}\right] - \frac{n^2\pi L}{2\sin^2\beta}\,(B_{22}+c_2) + \frac{\pi}{4}LB_{66}$$

$$L_{31} = \frac{m^3\pi^4}{L^3}B_{11}\sin\beta\left\{\frac{(x_0+L)^5-x_0^5}{10}+\frac{L^2\left[x_0^3-(x_0+L)^3\right]}{2m^2\pi^2}+\frac{3L^5}{4m^4\pi^4}\right\}$$
$$+\left[\frac{m^3\pi^4}{L^3}c_1^0\sin\beta+\frac{m\pi^2}{L}\cot\beta\sin\beta A_{12}\right]\left[\frac{(x_0+L)^4-x_0^4}{8}-\frac{3L^3\,(2x_0+L)}{8m^2\pi^2}\right]$$
$$+\left[\frac{m\pi^2}{L}\sin\beta\,(3B_{11}+B_{22}+c_2)+\frac{mn^2\pi^2}{L\sin\beta}\,(B_{12}+2B_{66})\right]\left[\frac{(x_0+L)^3-x_0^3}{6}-\frac{L^3}{4m^2\pi^2}\right]$$
$$+\cot\beta\sin\beta\left[A_{22}+\frac{E_{1r}b_r}{d_r}\right]\frac{L^2\,(2x_0+L)}{4m}+\frac{L^2}{4m}\sin\beta\,(B_{22}+c_2)\left[\frac{n^2}{\sin^2\beta}-1\right]$$

$$L_{32} = \frac{m^2n\pi^3}{L^2}\,(B_{12}+2B_{66})\left[\frac{(x_0+L)^4-x_0^4}{8}-\frac{3L^3\,(2x_0+L)}{8m^2\pi^2}\right]$$
$$+n\pi\cot\beta\left[A_{22}+\frac{E_{1r}b_r}{d_r}\right]\left[\frac{(x_0+L)^3-x_0^3}{6}-\frac{L^3}{4m^2\pi^2}\right]$$
$$+\frac{n\pi L\,(2x_0+L)}{4}\,(B_{22}+c_2)\left[\frac{n^2}{\sin^2\beta}-2\right]$$

$$L_{33} = -\frac{m^2\pi^3}{L^2}\cot\beta\sin\beta B_{12}\left[\frac{(x_0+L)^4-x_0^4}{8}-\frac{3L^3\,(2x_0+L)}{8m^2\pi^2}\right]$$
$$-\pi\cot^2\beta\sin\beta\left[A_{22}+\frac{E_{1r}b_r}{d_r}\right]\left[\frac{(x_0+L)^3-x_0^3}{6}-\frac{L^3}{4m^2\pi^2}\right]$$
$$-\frac{\pi}{4}L\,(2x_0+L)\cot\beta\sin\beta\,(B_{22}+c_2)\left[\frac{n^2}{\sin^2\beta}-2\right]$$

$$L_{34} = \frac{m^3\pi^4}{L^3}D_{11}\sin\beta\left\{\frac{(x_0+L)^5-x_0^5}{10}+\frac{L^2\left[x_0^3-(x_0+L)^3\right]}{2m^2\pi^2}+\frac{3L^5}{4m^4\pi^4}\right\}$$
$$+\left[\frac{m^3\pi^4}{L^3}\frac{E_{3s}b_s}{\lambda_0}\sin\beta+\frac{m\pi^2}{L}\cot\beta\sin\beta B_{12}\right]\left[\frac{(x_0+L)^4-x_0^4}{8}-\frac{3L^3\,(2x_0+L)}{8m^2\pi^2}\right]$$
$$+\left\{\frac{m\pi^2}{L}\sin\beta\left[3D_{11}+D_{22}+\frac{E_{3r}b_r}{d_r}\right]+\frac{mn^2\pi^2}{L\sin\beta}\,(D_{12}+2D_{66})\right\}\left[\frac{(x_0+L)^3-x_0^3}{6}-\frac{L^3}{4m^2\pi^2}\right]$$
$$+\frac{L^2\,(2x_0+L)}{4m}\cot\beta\sin\beta\,(B_{22}+c_2)+\frac{L^2}{4m}\sin\beta\left[D_{22}+\frac{E_{3r}b_r}{d_r}\right]\left[\frac{n^2}{\sin^2\beta}-1\right]$$

$$L_{35} = \frac{m^2n\pi^3}{L^2}\frac{1}{\sin\beta}\,(D_{12}+2D_{66})\left[\frac{(x_0+L)^3-x_0^3}{6}-\frac{L^3}{4m^2\pi^2}\right]$$
$$+\frac{n\pi}{4\sin\beta}L\,(2x_0+L)\cot\beta\,(B_{22}+c_2)-\frac{n\pi}{\sin\beta}L\,(D_{12}+2D_{66})$$
$$+\frac{n\pi}{2\sin\beta}L\left[D_{22}+\frac{E_{3r}b_r}{d_r}\right]\left[\frac{n^2}{\sin^2\beta}-2\right]-\frac{n\pi}{4\sin\beta}L\left(2D_{12}+D_{22}+4D_{66}+\frac{E_{3r}b_r}{d_r}\right)$$

$$L_{36} = -\frac{m^2\pi^3}{L^2}\sin\beta\left[\frac{(x_0+L)^4 - x_0^4}{8} - \frac{3L^3\,(2x_0+L)}{8m^2\pi^2}\right]$$

$$L_{37} = -\pi\sin\beta\left\{\frac{(x_0+L)^5 - x_0^5}{10} + \frac{L^2\left[x_0^3 - (x_0+L)^3\right]}{2m^2\pi^2} + \frac{3L^5}{4m^4\pi^4}\right\}$$

$$L_{38} = -\frac{m^2\pi^3}{L^2}\sin\beta\left\{\frac{(x_0+L)^5 - x_0^5}{10} + \frac{L^2\left[x_0^3 - (x_0+L)^3\right]}{2m^2\pi^2} + \frac{3L^5}{4m^4\pi^4}\right\}$$
$$-\frac{\pi}{2}\left[3\sin\beta + \frac{2n^2}{\sin\beta}\right]\left[\frac{(x_0+L)^3 - x_0^3}{6} + \frac{L^3}{4m^2\pi^2}\right]$$

$$L_{41} = -\frac{m^2\pi^3}{L^2}B_{11}\sin^2\beta\left[\frac{(x_0+L)^4 - x_0^4}{8} + \frac{3L^3\,(2x_0+L)}{8m^2\pi^2}\right]$$
$$-\frac{m^2\pi^3}{L^2}c_1^0\sin^2\beta\left[\frac{(x_0+L)^3 - x_0^3}{6} + \frac{L^3}{4m^2\pi^2}\right]$$
$$+\frac{\pi}{4}L\,(2x_0+L)\left[\sin^2\beta\,(B_{11} - B_{22} - c_2) - n^2B_{66}\right]$$

$$L_{42} = -\frac{mn\pi^2}{L}\sin\beta\,(B_{12}+B_{66})\left[\frac{(x_0+L)^3 - x_0^3}{6} + \frac{L^3}{4m^2\pi^2}\right] - \frac{nL^2}{4m}\sin\beta\,(B_{22}+B_{66}+c_2)$$

$$L_{43} = -\frac{m\pi^2}{L}A_{44}\sin^2\beta\left[\frac{(x_0+L)^4 - x_0^4}{8} + \frac{3L^3\,(2x_0+L)}{8m^2\pi^2}\right]$$
$$+\frac{m\pi^2}{L}\sin\beta\cos\beta B_{12}\left[\frac{(x_0+L)^3 - x_0^3}{6} + \frac{L^3}{4m^2\pi^2}\right] + \frac{L^2}{4m}\sin\beta\cos\beta\,(B_{22}+c_2)$$

$$L_{44} = -\left[\frac{m^2\pi^3}{L^2}D_{11}\sin^2\beta + \pi A_{44}\sin^2\beta\right]\left[\frac{(x_0+L)^4 - x_0^4}{8} + \frac{3L^3\,(2x_0+L)}{8m^2\pi^2}\right]$$
$$-\frac{m^2\pi^3}{L^2}\frac{E_{3s}b_s}{\lambda_0}\sin^2\beta\left[\frac{(x_0+L)^3 - x_0^3}{6} + \frac{L^3}{4m^2\pi^2}\right]$$
$$+\frac{\pi}{4}L\,(2x_0+L)\left\{\sin^2\beta\left[D_{11} - D_{22} - \frac{E_{3r}b_r}{d_r}\right] - n^2D_{66}\right\}$$

$$L_{45} = -\frac{mn\pi^2}{4}\,(2x_0+L)\,(D_{12}+D_{66})$$

$$L_{51} = -\frac{mn\pi^2}{L}\,(B_{12}+B_{66})\left[\frac{(x_0+L)^3 - x_0^3}{6} - \frac{L^3}{4m^2\pi^2}\right] - \frac{nL^2}{4m}\,(B_{22}+B_{66}+c_2)$$

$$L_{52} = -\frac{m^2\pi^3}{L^2}B_{66}\sin\beta\left[\frac{(x_0+L)^4 - x_0^4}{8} - \frac{3L^3\,(2x_0+L)}{8m^2\pi^2}\right]$$
$$-\frac{\pi}{2}L\,(2x_0+L)\left[\frac{n^2}{2\sin\beta}\,(B_{22}+c_2) + B_{66}\sin\beta\right]$$

$$L_{53} = -n\pi A_{55}\left[\frac{(x_0+L)^3 - x_0^3}{6} - \frac{L^3}{4m^2\pi^2}\right] + \frac{n\pi}{4}L\,(2x_0+L)\cot\beta\,(B_{22}+c_2)$$

$$L_{54} = -\frac{mn\pi^2}{L}\,(D_{12}+D_{66})\left[\frac{(x_0+L)^3 - x_0^3}{6} - \frac{L^3}{4m^2\pi^2}\right] - \frac{nL^2}{4m}\left[D_{22}+D_{66}+\frac{E_{3r}b_r}{d_r}\right]$$

$$L_{55} = -\pi\left[A_{55}+\frac{m^2\pi^2}{L^2}D_{66}\right]\left[\frac{(x_0+L)^3 - x_0^3}{6} - \frac{L^3}{4m^2\pi^2}\right] + \frac{\pi}{4}L\left\{D_{66} - \frac{2n^2}{\sin^2\beta}\left[D_{22}+\frac{E_{3r}b_r}{d_r}\right]\right\}$$

Funding

This research is funded by Vietnam National Foundation for Science and Technology Development (NAFOSTED) under grant number 107.02-2015.03. The authors are grateful for this support.

References

[1] M. Koizumi, "The concept of FGM, ceramic transactions," *Funct. Gradient. Mater.*, vol. 34, pp. 3–10, 1993.
[2] Y. L. Chung and H. X. Chang, "Mechanical behavior of rectangular plates with functionally graded coefficient of thermal expansion subjected to thermal loading," *J. Therm. Stresses*, vol. 31, no. 4, pp. 368–388, 2008.
[3] F. A. Fazzolari, "Modal characteristics of P- and S-FGM plates with temperature-dependent materials in thermal environment," *J. Therm. Stresses*, vol. 39, no. 7, pp. 854–873, 2016.
[4] W. H. Lee, S. C. Han, and W. T. Park, "A refined higher order shear and normal deformation theory for E-, P-, and S-FGM plates on Pasternak elastic foundation," *Compos. Struct.*, vol. 122, pp. 330–342, 2015.
[5] R. Naj, M. S. Boroujerdy, and M. R. Eslami, "Thermal and mechanical instability of functionally graded truncated conical shells," *Thin-Walled. Struct.*, vol. 46, pp. 65–78, 2008.
[6] D. H. Bich, N. T. Phuong, and H. V. Tung, "Buckling of functionally graded conical panels under mechanical loads," *Compos. Struct.*, vol. 94, pp. 1379–1384, 2012.
[7] E. Bagherizadeh, Y. Kiani, and M. R. Eslami, "Mechanical buckling of functionally graded material cylindrical shells surrounded by Pasternak elastic foundation," *Compos. Struct.*, vol. 93, pp. 063–071, 2011.
[8] J. Torabi, Y. Kiani, and M. R. Eslami, "Linear thermal buckling analysis of truncated hybrid FGM conical shells," *Compos. Part B*, vol. 50, pp. 265–272, 2013.
[9] J. E. Jam and Y. Kiani, "Buckling of pressurized functionally graded carbon nanotube reinforced conical shells," *Compos. Struct.*, vol. 125, pp. 586–595, 2015.
[10] M. Akbari, Y. Kiani, M. M. Aghdam, and M. R. Eslami, "Free vibration of FGM Lévy conical panels," *Compos. Struct.*, vol. 116, pp. 732–746, 2014.
[11] H. V. Tung, "Nonlinear thermomechanical stability of shear deformable FGM shallow spherical shells resting on elastic foundations with temperature dependent properties," *Compos. Struct.*, vol. 114, pp. 107–116, 2014.
[12] A. H. Sofiyev, "Thermoelastic stability of functionally graded truncated conical shells," *Compos. Struct.*, vol. 77, pp. 56–65, 2007.
[13] A. H. Sofiyev, "The buckling of FGM truncated conical shells subjected to combined axial tension and hydrostatic pressure," *Compos. Struct.*, vol. 92, pp. 488–498, 2010.
[14] A. H. Sofiyev, "Buckling analysis of freely-supported functionally graded truncated conical shells under external pressures," *Compos. Struct.*, vol. 132, pp. 746–758, 2015.
[15] A. H. Sofiyev, "The buckling of FGM truncated conical shells subjected to axial compressive load and resting on Winkler–Pasternak foundations," *Int. J. Press. Ves. Pip.*, vol. 87, pp. 753–761, 2010.
[16] T. Q. Quan and N. D. Duc, "Nonlinear thermal stability of eccentrically stiffened FGM double curved shallow shells," *J. Therm. Stresses*, vol. 40, pp. 211–236, 2016. DOI: 10.1080/01495739.2016.1225532
[17] B. Mirzavand, M. R. Eslami, and J. N. Reddy, "Dynamic thermal postbuckling analysis of shear deformable piezoelectric-FGM cylindrical shells," *J. Therm. Stresses*, vol. 36, no. 3, pp. 189–206, 2013.
[18] T. R. Mahapatra, V. R. Kar, S. K. Panda, and K. Mehar, "Nonlinear thermoelastic deflection of temperature-dependent FGM curved shallow shell under nonlinear thermal loading," *J. Therm. Stresses*, vol. 40, pp. 1184–1199, 2017. DOI: 10.1080/01495739.2017.1302788
[19] A. H. Sofiyev and N. Kuruoglu, "Nonlinear buckling of an FGM truncated conical shells surrounded by an elastic medium," *Int. J. Press. Ves. Pip.*, vol. 107, pp. 38–49, 2013.
[20] A. H. Sofiyev and N. Kuruoglu, "The stability of FGM truncated conical shells under combined axial and external mechanical loads in the framework of the shear deformation theory," *Compos. Part B*, vol. 92, pp. 463–476, 2016.

[21] F. Tornabene and E. Viola, "Static analysis of functionally graded doubly-curved shells and panels of revolution," *Meccanica*, vol. 48, pp. 901–930, 2013.
[22] F. Tornabene, N. Fantuzzi, E. Viola, and R. C. Batra, "Stress and strain recovery for functionally graded free-form and doubly-curved sandwich shells using higher-order equivalent single layer theory," *Compos. Struct.*, vol. 119, pp. 67–89, 2015.
[23] E. Viola, L. Rossetti, N. Fantuzzi, and F. Tornabene, "Static analysis of functionally graded conical shells and panels using the generalized unconstrained third order theory coupled with the stress recovery," *Compos. Struct.*, vol. 112, pp. 44–65, 2014.
[24] M. Z. Nejad, M. Jabbari, and M. Ghannad, "Elastic analysis of FGM rotating thick truncated conical shells with axially-varying properties under non-uniform pressure loading," *Compos. Struct.*, vol. 122, pp. 561–569, 2015.
[25] Z. Mecitoglu, "Vibration characteristics of a stiffened conical shell," *J. Sound Vib.*, vol. 197(2), pp. 191–206, 1996.
[26] S. S. Rao and E. S. Reddy, "Optimum design of stiffened conical shells with natural frequency constraints," *Compos. Struct.*, vol. 14, no. 1–2, pp. 103–110, 1981.
[27] E. Bagherizadeh, Y. Kiani, and M. R. Eslami, "Thermal buckling of functionally graded material cylindrical shells on elastic foundation," *AIAA. J.*, vol. 50, pp. 500–503, 2012.
[28] M. Akbari, Y. Kiani, and M. R. Eslami, "Thermal buckling of temperature-dependent FGM conical shells with arbitrary edge supports," *Act. Mech.*, vol. 226, pp. 897–915, 2015.
[29] M. Mirzaei and Y. Kiani, "Thermal buckling of temperature dependent FG-CNT reinforced composite conical shells," *Aer. Sci. Tech.*, vol. 47, pp. 42–53, 2015.
[30] M. Sabzikar Boroujerdy, R. Naj, and Y. Kiani, "Buckling of heated temperature dependent FGM cylindrical shell surrounded by elastic medium," *Theor. Appl. Mech.*, vol. 52, pp. 869–881, 2014.
[31] H. Asadi, Y. Kiani, M .M. Aghdam, and M. Shakeri, "Enhanced thermal buckling of laminated composite cylindrical shells with shape memory alloy," *J. Compos. Mater.*, vol. 50, pp. 243–256, 2015.
[32] S. Castro, C. Mittelstedt, F. A. C. Monteiro, M. A. Arbelo, G. Ziegmann, and R. Degenhardt, "Linear buckling predictions of unstiffened laminated composite cylinders and cones under various loading and boundary conditions using semi-analytical models," *Compos. Struct.*, vol. 118, pp. 303–315, 2014.
[33] S. Castro, C. Mittelstedt, F. A. C. Monteiro, M. A. Arbelo, G. Ziegmann, and R. Degenhardt, "A semi-analytical approach for the linear and non-linear buckling analysis of imperfect unstiffened laminated composite cylinders and cones under axial, torsion and pressure loads," *Thin-Wall. Struct.*, vol. 90, pp. 61–73, 2015.
[34] M. M. Najafizadeh, A. Hasani, and P. Khazaeinejad, "Mechanical stability of functionally graded stiffened cylindrical shells," *Appl. Math. Model.*, vol. 33, pp. 1151–1157, 2009.
[35] N. D. Duc and T. Q. Quan, "Nonlinear postbuckling of imperfect eccentrically stiffened PFGM double curved thin shallow shells on elastic foundations in thermal environments," *J. Compos Struct.*, vol. 106, pp. 590–600, 2013.
[36] D. V. Dung and V. H. Nam, "Nonlinear dynamic analysis of eccentrically stiffened functionally graded circular cylindrical thin shells under external pressure and surrounded by an elastic medium," *Eur. J. Mech. A Solids*, vol. 46, pp. 42–53, 2014.
[37] D. V. Dung and L. K. Hoa, "Research on nonlinear torsional buckling and post-buckling of eccentrically stiffened FGM cylindrical shell in thermal environment," *Compos Part B Eng.*, vol. 69, pp. 378–388, 2015.
[38] N. D. Duc, "Nonlinear thermal dynamic analysis of eccentrically stiffened S-FGM circular cylindrical shells surrounded on elastic foundations using the Reddy's third-order shear deformation shell theory," *Eur. J. Mech. A Solids*, vol. 58, pp. 10–30, 2016.
[39] N. D. Duc, P. D. Nguyen, and N. D. Khoa, "Nonlinear dynamic analysis and vibration of eccentrically stiffened S-FGM elliptical cylindrical shells surrounded on elastic foundations in thermal environments," *Thin-Wall. Struct.*, vol. 117, pp. 178–189, 2017.
[40] D. V. Dung, L. K. Hoa, N. T. Nga, and L. T. N. Anh, "Instability of eccentrically stiffened functionally graded truncated conical shells under mechanical loads," *Compos. Struct.*, vol. 106, pp. 104–113, 2013.
[41] D. V. Dung, L. K. Hoa, B. T. Thuyet, and N. T. Nga, "Buckling analysis of functionally graded material (FGM) sandwich truncated conical shells reinforced by FGM stiffeners filled inside by elastic foundations," *App. Math. Mech. (Eng Edit)*, vol. 37(7), pp. 879–902, 2016.
[42] N. D. Duc and P. H. Cong, "Nonlinear thermal stability of eccentrically stiffened functionally graded conical shells surrounded on elastic foundations," *Eur. J. Mech. A Solids*, vol. 50, pp. 120–131, 2015.
[43] N. D. Duc, P. H. Cong, V. M. Anh, V. D. Quang, T. Phuong, N. D. Tuan, and N. H. Thinh, "Mechanical and thermal stability of eccentrically stiffened functionally graded conical shell panels resting on elastic foundations and in thermal environment," *Compos. Struct.*, vol. 132, pp. 597–609, 2015.
[44] K. M. Liew, J. Yang, and Y. F. Wu, "Nonlinear vibration of a coating-FGM-substrate cylindrical panel subjected to a temperature gradient," *Comput. Meth. App. Mech. Eng.*, vol. 195, pp. 1007–1026, 2016.
[45] A. Alibeigloo and K. M. Liew, "Free vibration analysis of sandwich cylindrical panel with functionally grade core using three-dimensional theory of elasticity," *Compos. Struct.*, vol. 113, pp. 23–30, 2014.
[46] S. R. Li and R. C. Batra, "Buckling of axially compressed thin cylindrical shells with functionally graded middle layer," *Thin-Wall. Struct.*, vol. 44, pp. 1039–1047, 2006.

[47] A. H. Sofiyev and N. Kuruoglu, "Torsional vibration and buckling of the cylindrical shell with functionally graded coatings surrounded by an elastic medium," *Compos Part B*, vol. 45, pp. 1133–1142, 2013.
[48] A. H. Sofiyev, "The vibration and buckling of sandwich cylindrical shells covered by different coatings subjected to the hydrostatic pressure," *Compos. Struct.*, vol. 117, pp. 124–134, 2014.
[49] A. M. Najafov, A. H. Sofiyev, and N. Kuruoglu, "On the solution of nonlinear vibration of truncated conical shells covered by functionally graded coatings," *Act. Mech.*, vol. 225, pp. 563–580, 2014.
[50] A. H. Sofiyev, Z. Zerin, and A. Korkmaz, "The stability of a thin three-layered composite truncated conical shell containing an FGM layer subjected to non-uniform lateral pressure," *Compos. Struct.*, vol. 85, pp. 105–115, 2008.
[51] A. Deniz, "Nonlinear stability analysis of truncated conical shell with functionally graded composite coatings in the finite deflection," *Compos. Part B*, vol. 51, pp. 318–326, 2013.
[52] A. H. Sofiyev, "On the dynamic buckling of truncated conical shells with functionally grade coatings subjected to a time dependent axial load in the large deformation," *Compos. Part B*, vol. 58, pp. 524–533, 2014.
[53] J. Seidi, S. M. R. Khalili, and K. Malekzadeh, "Temperature-dependent buckling analysis of sandwich truncated conical shells with FG facesheets," *Compos. Struct.*, vol. 131, pp. 682–691, 2015.
[54] N. D. Duc, "Nonlinear thermo-electro-mechanical dynamic response of shear deformable piezoelectric sigmoid functionally graded sandwich circular cylindrical shells on elastic foundations," *J. Sandwich. Struct. Mater.*, 2016. DOI:10.1177/1099636216653266
[55] N. D. Duc and T. Q. Quan, "Nonlinear dynamic analysis of imperfect FGM double curved thin shallow shells with temperature-dependent properties on elastic foundation," *J. Vib. Control.*, vol. 21, no. 7, pp. 1340–1362, 2015.
[56] T. Q. Quan and N. D. Duc, "Nonlinear vibration and dynamic response of shear deformable imperfect functionally graded double curved shallow shells resting on elastic foundations in thermal environments," *J. Therm. Stresses*, vol. 39, no. 4, pp. 437–459, 2016.
[57] D. O. Brush and B. O. Almorth, *Buckling of Bars, Plates and Shells*. New York: McGraw-Hill, 1975.
[58] C. S. Xu, Z. Q. Xia, and C. Y. Chia, "Nonlinear theory and vibration analysis of laminated truncated thick conical shells," *Int. J. Non-Linear. Mech.*, vol. 31, no. 2, pp. 39–54, 1996.
[59] L. Tong and T. K. Wang, "Simple solutions for buckling of laminated conical shells," *Int. J. Mech. Sci.*, vol. 34, no. 2, pp. 93–111, 1992.
[60] A. S. Volmir, *The Stability of Deformable Systems*. Moscow: Nauka, 1967 (in Russian).
[61] M. Baruch, O. Harari, and J. Singer, "Low buckling loads of axially compressed conical shells," *J. Appl. Mech.*, vol. 37, pp. 384–392, 1970.